The impact of ventilation patterns on calcite dissolution rates within karst conduits

Matthew D. Covington[a,b], Katherine J. Knierim[c], Holly A. Young[a], Josue Rodriguez[a], Hannah G. Gnoza[a]

[a] *Department of Geosciences, University of Arkansas, Fayetteville, Arkansas, USA*
[b] *Karst Research Institute, ZRC SAZU, Slovenia*
[c] *U. S. Geological Survey, Lower Mississippi-Gulf Water Science Center*

Abstract

Erosion rates in streams vary dramatically over time, as differences in streamflow and sediment load enhance or inhibit erosion processes. Within cave streams, and other bedrock channels incising soluble rocks, changes in water chemistry are an important factor in determining how erosion rates will vary in both time and space. Prior studies in surface streams, springs, and caves suggest that variation in dissolved CO_2 is the strongest control on variation in calcite dissolution rates. However, the controls on CO_2 variation remain poorly quantified. Limited data suggest that ventilation of karst systems can substantially influence dissolved CO_2 within karst conduits. However, the interactions among cave ventilation, air-water CO_2 exchange, and dissolution dynamics have not been studied in detail. In this study, three years of time series measurements of dissolved and gaseous CO_2, cave airflow velocity, and specific conductance from Blowing Springs Cave, Arkansas, were analyzed and used to estimate continuous calcite dissolution rates and quantify the correlations between those rates and potential physical and chemical drivers. We find that chimney effect airflow creates temperature-driven switches in airflow direction, and that the resulting seasonal changes in airflow regulate both gaseous and dissolved CO_2 within the cave. As in previous studies, partial pressure of CO_2 (pCO_2) is the strongest chemical control of dissolution rate variability. However, we also show that cave airflow direction, rather than streamflow, is the strongest physical driver of changes in dissolution rate, contrary to the typical situation in surface channel erosion where floods largely determine the timing and extent of geomorphic work. At the study site, chemical erosion is typically active in the summer, during periods

of cave downdraft (airflow from upper to lower entrances), and inactive in the winter, during updraft (airflow from lower to upper entrances). Storms provide only minor perturbations to this overall pattern. We also find that airflow direction modulates dissolution rate variation during storms, with higher storm variability during updraft than during downdraft. Finally, we compare our results with the limited set of other studies that have examined dissolution rate variation within cave streams and draw an initial hypothesis that evolution of cave ventilation patterns strongly impacts how dissolution rate dynamics evolve over the lifetime of karst conduits.

Keywords:
karst, bedrock channel, cave ventilation, carbon dioxide, dissolution

---

1. Introduction

The variation in geomorphic rates has an important influence on the relationship between erosional processes and the landforms that they produce (Wolman and Miller, 1960). Whereas concepts of the magnitude and frequency of geomorphic work have long been explored in the study of processes on Earth's surface, fewer studies have examined the variability in rates of cave development or the factors that control this variation (Groves and Meiman, 2005). Cave passages are often developed by subsurface streams incising through bedrock. Since many cave streams carry substantial sediment loads (Farrant and Smart, 2011), mechanical erosion processes, such as occur within surface bedrock channels (Whipple et al., 2000), undoubtedly are active within these streams. However, most caves develop in karst settings, within highly soluble rocks, where chemical dissolution of the rock is an important driver of channel development and evolution (Ford and Williams, 2007; Palmer, 2007a).

A number of studies have measured solute export from basins and used these data to examine how rates of chemical denudation vary with streamflow (Wolman and Miller, 1960; Gunn, 1982; Schmidt, 1985; Goudie and Viles, 1999). These studies conclude that low to moderate flows produce an important percentage of the overall chemical geomorphic work at the basin scale. However, rates of channel incision by dissolution and basin-wide chemical denudation do not in general display the same relationship to streamflow. Groves and Meiman (2005) show that, in the Logsdon River passage of Mammoth Cave, Kentucky, conduit wall dissolution rates are a strong function of

discharge, with 87% of the work being done during high discharges that occur less than 5% of the time. In contrast, they find that solute export is important across a range of discharges, with only 38% of the export occurring during the highest discharge class. Palmer (2007b) finds a similar relationship between discharge and calcite dissolution rate in McFail's Cave, New York. Analysis of water chemistry data from streams across the United States suggests that variability in calcite dissolution rates at most sites is more strongly correlated with variability in dissolved CO_2 than with streamflow, and that in-channel dissolution rates are often much higher than estimates of basin-wide denudation rates (Covington et al., 2015). Covington and Vaughn (2019) show that seasonal variability in CO_2 is the primary driver for variation in calcite dissolution rates at a pair of karst underflow-overflow springs. Additionally, they hypothesize that, during low flows, ventilation within the conduit feeding the overflow spring drives a reduction in CO_2 and, consequently, dissolution rates. In general, previous investigators have argued that cave ventilation, which often occurs in the later stages of cave development, may reduce the rates of chemical erosion within cave streams as caves becomes more mature (Palmer, 2007b).

While it is clear that both floods and CO_2 dynamics are important drivers of dissolution rate variability within cave streams, there are relatively few cave sites where dissolution rate variability has been quantified (Groves and Meiman, 2005; Palmer, 2007b; Covington and Vaughn, 2019). This lack of data limits the ability to generalize about the controls on calcite dissolution rate variability. Here, we analyze water chemistry data in a cave stream in the Ozark Plateaus physiographic region of Arkansas to explore potential controls of dissolution rate variability. We use recently developed techniques for direct, high temporal resolution measurements of dissolved CO_2 (Johnson et al., 2010), combined with time series of specific conductance (SpC), to estimate calcite dissolution rates over a three-year period. These measurements are complemented by simultaneous measurements of cave air CO_2 and cave airflow velocity. This enables us to explore interactions between cave atmosphere dynamics and cave stream chemistry.

2. Description of field site

Blowing Springs Cave is located in Bella Vista, Arkansas, within the Springfield Plateau region of the Ozark Plateaus (Figure 1). The cave is developed in the cherty Mississippian Boone Limestone primarily within the

St. Joe Limestone Member (McFarland, 1998). Because of a high concentration of chert and clay impurities, the Boone Limestone develops a mantled karst, where a thick regolith composed of chert and clay covers the karst surface (Brahana, 2011). Within the region surrounding the cave, the Boone Limestone spans the topography from valley floors to ridges. The cave, therefore, is autogenically recharged through a regolith cover. Because of the regolith cover, the region contains few obvious surface karst features, such as sinkholes, though most of the valleys located in the recharge area are dry except during periods of intense precipitation. The land cover in the recharge area is a mixture of deciduous forest and low intensity residential. The region has a temperate continental climate with a mean annual air temperature of approximately 15°C (Adamski et al., 1995) and a mean annual precipitation of about 114 centimeters per year (cm/yr) (Pugh and Westerman, 2014).

Blowing Springs Cave contains 2,397 meters (m) of mapped cave passage and consists of a dendritic stream network (Figure 1). Water enters the main cave stream through a number of small infeeding channels and through many percolating fractures within the cave ceiling, though the largest source of discharge to the cave stream is the upstream sump. Many of the cave passages are oriented along an orthogonal set of NE-SW and NW-SE trending fractures. The only known entrance of the cave is at the spring, and, as the name suggests, the cave exhibits strong airflow, with air blowing out of the spring entrance during times of warm outside temperatures. The spring emerges near the elevation of the local base-level stream, which is Little Sugar Creek.

3. Methods

3.1. Collection of time series data

Time series data of water quality and cave atmospheric parameters were collected at a site located approximately 150 m inside the cave entrance, which is labeled as Cave Measurement Station in Figure 1. Cave airflow velocity, cave air barometric pressure, and CO_2 concentrations in the cave air and water were logged on a Campbell Scientific^{TM}CR850 datalogger. Cave airflow velocity and direction were measured using a Campbell Scientific WINDSONIC1 2D ultrasonic anemometer (resolution 0.01 m/s; accuracy $\pm 2\%$ at 12 m/s; directional accuracy $\pm 3°$). Barometric pressure was measured using a Campbell Scientific^{TM}CS100 sensor (accuracy ± 0.5 hPa). CO_2 concentrations in the air and water were measured using Vaisala GMM220

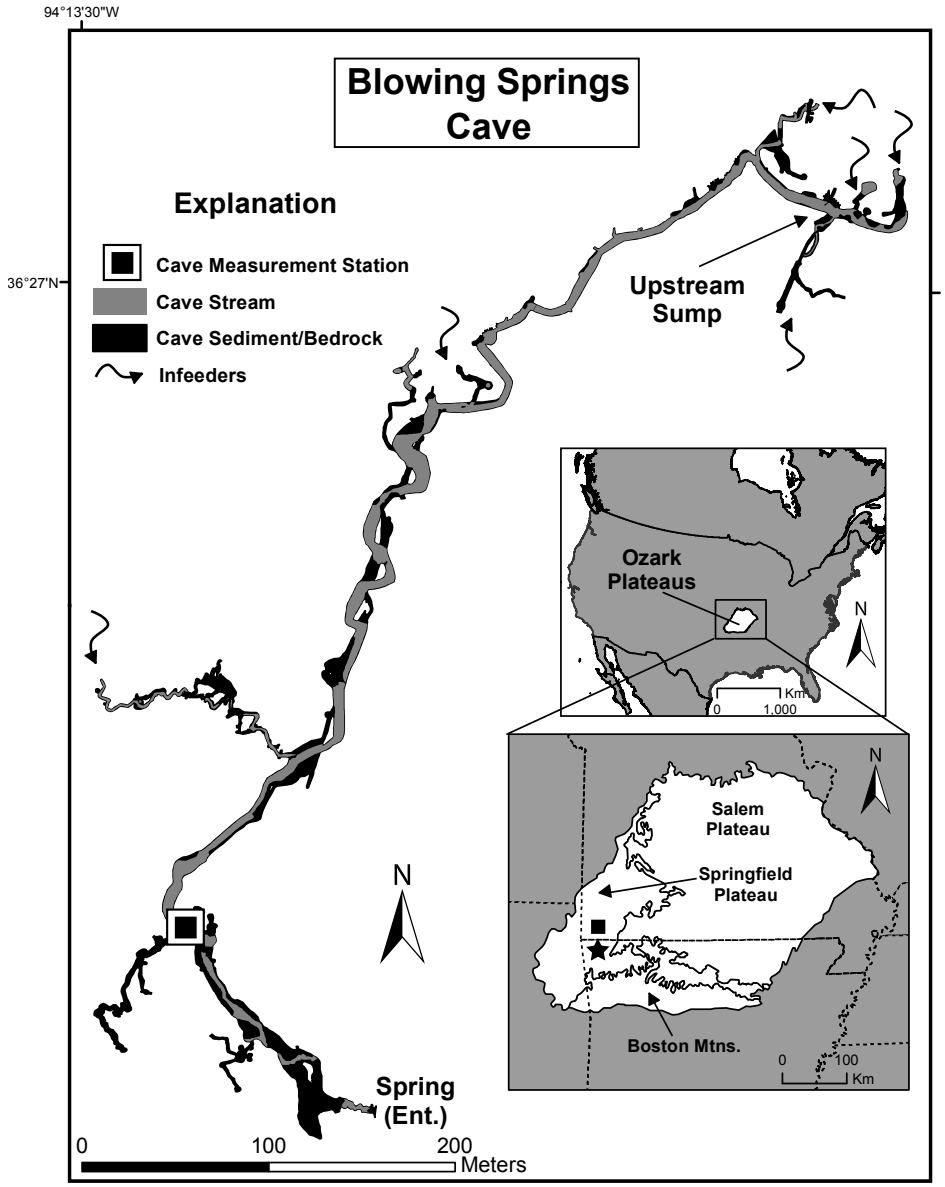

Figure 1: Location of Blowing Springs Cave (star) and map of the cave depicting the entrance, measurement location, stream, and upstream sump. Within the inset, the square indicates the location of the USGS stream gauge on Little Sugar Creek (USGS station no. 07188838). Modified from Knierim et al. (2017). Original cave map and survey data from Covington (2007).

CO_2 transmitters with a range of 0 to 5,000 parts per million (ppm) (accuracy $\pm 1.5\%$ of range $\pm 2\%$ of reading). The CO_2 sensors were protected from moisture with a waterproof breathable membrane (PTFE) as described in Johnson et al. (2010). One sensor was exposed to the cave air, and the other was submerged in the cave stream to enable direct measurement of the partial pressure of CO_2 (pCO_2) of the water. This setup provides a more reliable means of recording pCO_2 than continuous measurement of pH, as the CO_2 sensors exhibit much less drift over time than pH electrodes (Johnson et al., 2010; Covington and Vaughn, 2019). For the CO_2 sensors, a warm-up period of 15 minutes was used before a measurement was taken. This warm-up period allowed thermal equilibration of the sensor and helped to drive any moisture out of the sensor optics. We found that this warm-up period was crucial, as substantial instrument drift occurred within the first few minutes of power-up. Measured values of pCO_2 were not adjusted with water depth as described by (Johnson et al., 2010), because subsequent theoretical analysis and experiments have shown that this adjustment is incorrect (Blackstock et al., 2019). CO_2 readings were taken once an hour to conserve power, whereas other parameters recorded on the CR850 were read on a one-minute interval.

In this study, all CO_2 concentrations are reported in ppm, which are nominally values of ppm volume (ppmV) within a gas phase, where the concentrations for our dissolved measurements are within a headspace equilibrated to the dissolved phase. Air and water values are reported in the same units to enable direct comparison, and use ppm as these are the units typically used in cave atmospheric studies. While the instrument reports ppmV, it actually directly measures molecular density. Concentrations in ppmV must be corrected both for pressure and temperature. We are specifically interested in pCO_2, which can be more directly calculated from molecular density than can ppmV, only requiring a temperature correction and the factory calibration pressure (Blackstock et al., 2019), which we assume to be 1 atm. We apply the temperature correction, and then 1 ppm is equivalent to a pCO_2 of 10^{-6} atm. Therefore, our reported ppm values are directly proportional to pCO_2 and can be thought of as a type of pCO2 value, albeit with unusual units.

The specific conductance (SpC) and temperature of the cave stream were measured at the same site as CO_2 on a time interval of 5 minutes using an Onset HOBO^{TM}U24-001 freshwater conductivity logger with an accuracy of 3% or 5 microsiemens per centimeter (μS/cm). Outside of the cave, air tem-

perature and relative humidity were measured at a 5-minute interval using an Onset HOBO^{TM}U23-001 temperature (accuracy $\pm 0.21°C$) and relative humidity (accuracy $\pm 2.5\%$) logger that was mounted onto a tree. To provide a proxy for stable cave temperature, we deployed an Onset HOBO^{TM}U20L-04 pressure and temperature logger in the cave air approximately 400 m inside the cave (accuracy $\pm 0.44°C$). Unless specified otherwise, all data presented here are hourly averages, to align with the frequency of CO_2 measurements.

The site within the cave was visited roughly every four weeks, which was the approximate duration of the battery power supply (two 12-volt, 20 Amp-hour lithium-ion batteries). During each site visit, batteries were changed, data downloaded, and quality control on-site measurements were made of specific conductance, water temperature, and CO_2 concentrations in the air and water. To make on-site measurements of CO_2 a portable Vaisala GMM220 was used that was connected to a battery and data logger. Spot measurements of CO_2 in the water required a roughly 30-minute equilibration period for gas concentrations to exchange across the PTFE membrane.

Whereas a partial record of stage and estimated discharge is available at the spring, frequent human disturbances of the stream channel near the weir (the site is located in a park) reduced the quality of the available dataset. Rather than using this corrupted record, we employ a modification of an estimation of discharge at Blowing Springs Cave developed by Knierim et al. (2015b) using the nearby United States Geological Survey (USGS) streamflow-gaging station on Little Sugar Creek (USGS Station no. 07188838 Little Sugar Creek near Pineville, Missouri) with data available from the USGS National Water Information System (U.S. Geological Survey, 2020).

Knierim et al. (2015b) found that a linear regression provided a reasonable approximation of discharge at Blowing Springs. However, they also noted that Blowing Springs exhibited a minimum baseflow discharge, and therefore they introduced a threshold minimum value. To remove the sharp threshold and reduce errors on moderate discharge values, we introduce a new regression to daily averaged discharges using a sigmoidal function in log space (Figure 2),

$$\log(Q_{\mathrm{BSC}}) = \frac{A}{1 + \exp(-D[\log(Q_{\mathrm{LSC}}) - B])} + C, \tag{1}$$

where Q_{BSC} is the discharge at Blowing Springs in m^3/s and Q_{LSC} is the streamflow in Little Sugar Creek, and the best fit values of the fitting pa-

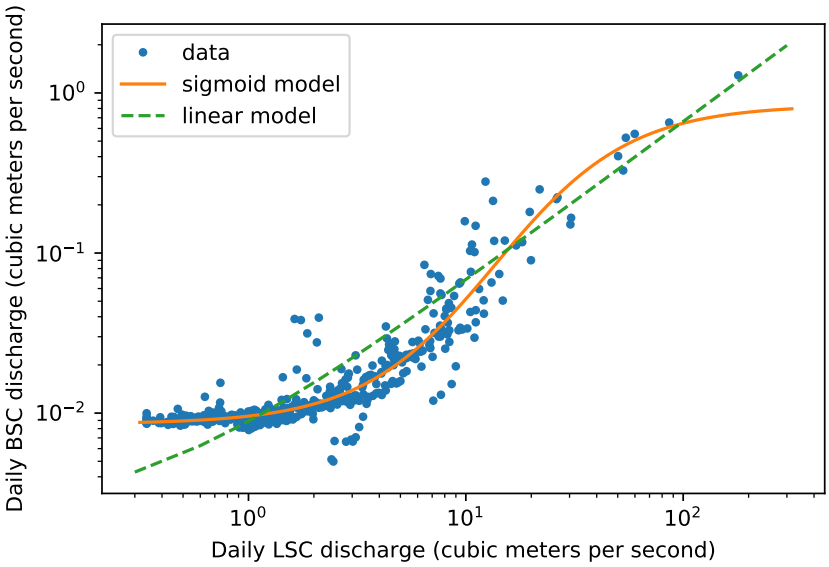

Figure 2: Regression used in the estimation of Blowing Springs discharge from the stream gauge at Little Sugar Creek. The sigmoid model is used in this work, and the linear model is from Knierim et al. (2015b).

rameters are $A = 1.99$, $B = 1.14$, $C = -2.07$, and $D = 3.24$. The root mean squared percentage error (RMSPE) in this model is 33%. The sigmoidal shape nicely captures the transition to baseflow and also captures a possible rolloff at high discharges ($\sim 1 - 2$ m^3/s) that is evident in the 15-minute data. Many karst springs do exhibit maximum discharges (Bonacci, 2001), though this upper rolloff also has limited impact on our estimates due to the small number of data points that fall at these highest discharges. Most of our results are independent of this discharge estimate, which is primarily used to indicate the occurrence and frequency of high and low flow periods to examine how dissolution rate varies with flow. The precise magnitudes of discharge are not necessary for interpreting our data.

3.2. Calculation of dissolution rates

In order to calculate dissolution rates from available kinetic rate equations, we need values for the dissolved Ca concentration and the pCO_2. While we measure pCO_2 directly, Ca concentrations were estimated from SpC time

series collected at the site, as has also been done in prior studies of dissolution rate dynamics within karst systems (Groves and Meiman, 2005; Covington and Vaughn, 2019) and is appropriate where water is predominantly Ca–HCO_3 type. To estimate Ca, we use a linear regression on available SpC and Ca data ($n = 109$) from a prior study at Blowing Springs Cave (Knierim et al., 2017). We find that $[\mathrm{Ca}] = 0.175 \times \mathrm{SpC} - 2.51$, where [Ca] is concentration in mg/L. The RMSPE of this relationship is 10%. However, uncertainties are larger for lower SpC values. Therefore, for error propagation purposes we divide the data into quartiles and use separate uncertainty values for each quartile, these uncertainties range from 4.5% to 13.7%. These data and further details on error estimation can be found in the data repository described in the Data Availability section of this paper.

To calculate dissolution rates from [Ca] and pCO_2 time series, we use two available calcite kinetic equations, which we refer to as the PWP (Plummer et al., 1978) and Palmer equations (Palmer, 1991). Both equations are derived from the same experimental dataset, but the Palmer equation is a direct fit to the data, whereas the PWP equation incorporates a more mechanistic approach to parameter estimation. The Palmer equation generates a closer fit to the observed dissolution rates near saturation and also provides parameter values for impure calcite, which is more appropriate for limestone. Covington and Vaughn (2019) found that the Palmer equation provided much closer estimates of mass loss rates of limestone tablets deployed in the field, and therefore, it is likely that these rates are more accurate in natural settings.

The PWP equation sometimes produces negative rates, which might suggest calcite precipitation. However, calcite precipitation normally does not occur until waters are highly supersaturated, therefore negative PWP rates are not necessarily indicative of precipitation. In time series of dissolution rates, we show both the PWP and Palmer equations. However, when studying sensitivity of rates to various potential controls, it is helpful to have a broader range of values, including a range of negative values that represent different extents of supersaturation. Therefore, we use PWP rates to explore controls on variability, even though the magnitude of the rates is likely too high (Covington and Vaughn, 2019). Rates predicted by both equations typically vary monotonically with one another. Both dissolution rate equations were calculated using algorithms in the *Olm* Python package v0.36 (Covington et al., 2015), which is available on *Github* (`https://doi.org/10.5281/zenodo.4030690`). Uncertainties in dissolution rates were estimated using Monte Carlo error propagation from uncertainties

in [Ca] and pCO_2.

4. Results

4.1. Large-scale patterns in the time series data

The water chemistry and cave atmosphere parameters were recorded over a period of approximately three years (Oct. 2014-Jan. 2018). CO_2 concentrations in air and water range between near atmospheric concentration (≈500 ppm) to above 5,000 ppm (Figure 3a). For a few short periods, pCO_2 in the water exceeded the measurement range of the sensor deployed (≈5,500 ppm). Concentrations in the water almost always exceeded those in the air. Both dissolved and gaseous CO_2 concentrations within the cave showed seasonal patterns, with higher concentrations in summer and lower concentrations during winter. Gaseous CO_2 within the cave dropped near atmospheric values for much of the winter. Dissolved CO_2 often exhibited spikes to higher values associated with high discharge events. Gaseous CO_2 displayed strong diurnal variability during certain periods, particularly during the spring and fall. These periods of variability are associated with times when outside air temperatures are near those of the cave air temperature, which is approximately the mean surface air temperature (Badino, 2010).

Cave airflow velocity also had a seasonal pattern with outward (positive) airflow during warm periods and inward (negative) airflow during cold periods (Figure 3b). There was diurnal variability in airflow velocity, particularly during spring and fall periods, with some days exhibiting both inward and outward airflow at different times of day. Again, these periods of high variability are times when outside temperatures are near the temperature of the cave atmosphere.

Specific conductance displayed a range from 65 to 265 μS/cm. Variability in SpC was more strongly related to discharge than to season (Figures 3c,d). SpC was high during periods of low flow and low during periods of high flow, particularly flood events. All records display gaps that are associated with sensor or power failures. However, the SpC record is the least complete, with a large number of gaps resulting from sensor failure, damage during storms, or download failure, which lead to memory filling on the datalogger before the next opportunity to download. As can be seen visually in Figures 3c,d, there is a strong correlation between specific conductance and stream discharge (Q). The relationship between these parameters is explicitly displayed in

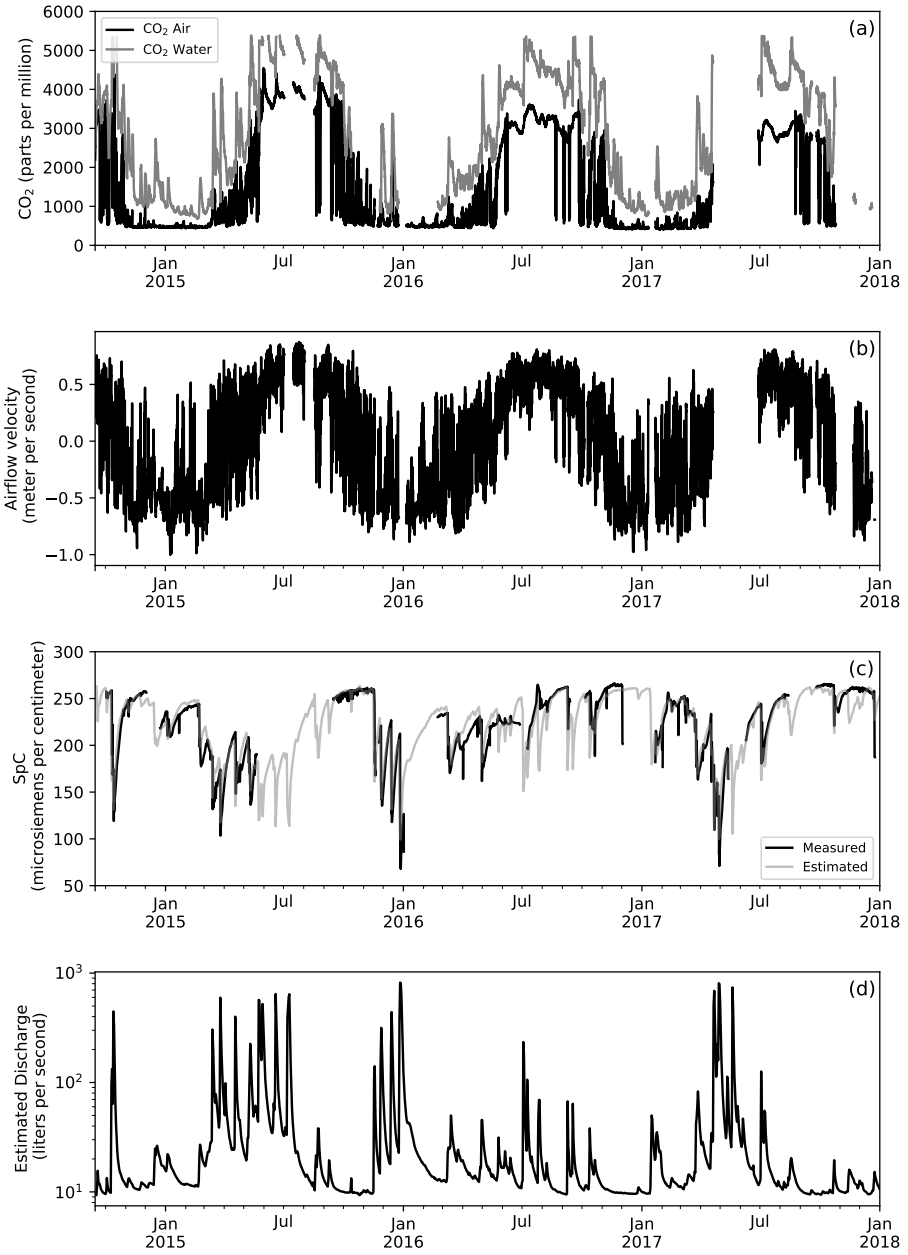

Figure 3: Time series data for the entire study period: (a) CO_2 concentrations in the air and water, (b) cave airflow velocity (positive values indicate the cave is blowing out), (c) specific conductance in the cave stream (black) and an estimated daily specific conductance using a regression to discharge (gray), and (d) estimated discharge of the cave calculated from streamflow at Little Sugar Creek using Equation 1.

Figure 4 along with a 4th-order polynomial regression between $\log(Q)$ and specific conductance given by

$$\mathrm{SpC} = Ax^4 + Bx^3 + Cx^2 + D, \tag{2}$$

where $x = \log(Q)$, $A = -48.6$, $B = 296.2$, $C = -639.4$, and $D = 649.2$. The coefficients were determined using the *polyfit()* function from the *NumPy* package in Python. Because of the large number of gaps, and the strong relationship between discharge and SpC, the daily estimated SpC using Equation 2 is shown in Figure 3c. The root-mean-squared error (RMSE) in estimated SpC is 14.9 μS/cm. The valid discharge range for the fit is from approximately 10 L/s to 1,000 L/s. During periods where SpC data were lacking, we estimate [Ca] from these modeled values. To account for additional uncertainty introduced by this step, we divide these data into 10 percentile-based bins of discharge and calculate the RMSE for each of these bins. We use Gaussian Error Propagation to convert these uncertainties in SpC into uncertainty in [Ca].

4.2. Relationship between cave airflow and external air temperature

The seasonal and diurnal patterns in cave airflow velocity suggest a relationship between outside air temperature and cave airflow, as would be expected in the case of chimney effect airflow (Wigley and Brown, 1976; Luetscher et al., 2008; Badino, 2010; Covington and Perne, 2015). Chimney effect airflow is an airflow mechanism driven by density contrasts between the cave air and outside air and occurs within cave systems with more than one opening to the outside. During periods of warm outside temperatures, cave air is more dense than outside air and it is therefore pushed from upper entrances to lower entrances. During cold outside temperatures, cave air is less dense than outside air and rises from lower entrances to upper entrances. Note that such airflow does not require human-sized entrances or large elevation differences. Millimeter-scale fracture apertures and decimeters of elevation difference are sufficient (Covington, 2016).

The pressure difference, ΔP, that drives chimney effect airflow can be approximated using (cf. Badino (2010))

$$\Delta P = \rho_{\mathrm{in}} g h \frac{\Delta T}{T_{\mathrm{ext}}}, \tag{3}$$

where ρ_{in} is the density of the air inside the cave, g is Earth's gravitational acceleration, h is the height difference between the two entrances, ΔT is the

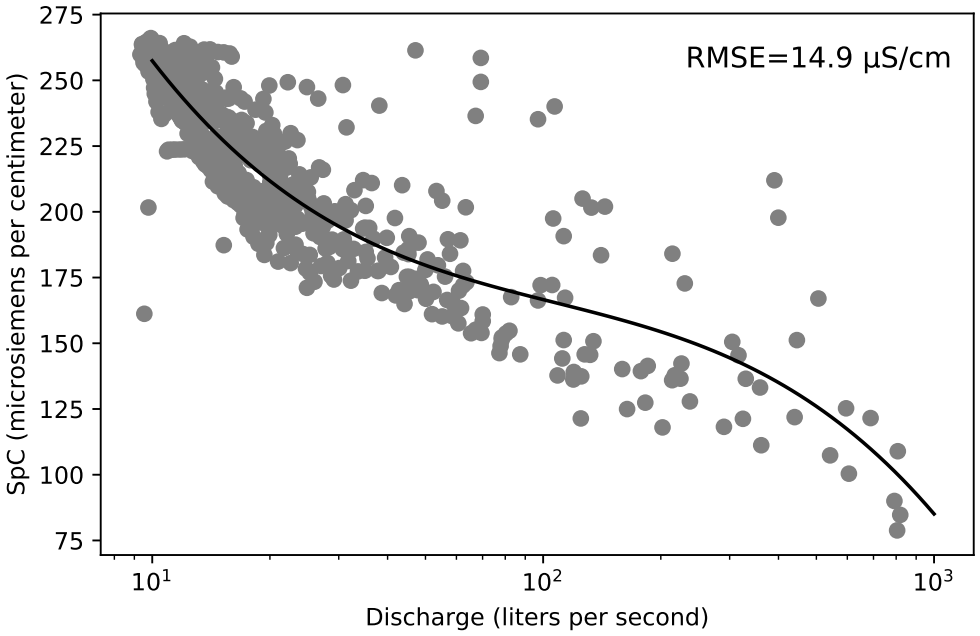

Figure 4: Relationship between specific conductance and discharge shown along with the polynomial regression (Equation 2) used for estimating specific conductance during periods of missing record (RMSE=root-mean-squared error).

difference between cave and external temperature, and T_{ext} is the external air temperature in Kelvin. Chimney effect airflow is typically turbulent, and therefore the Darcy–Weisbach equation for flow of fluid in a pipe provides a reasonable approximation (Luetscher and Jeannin, 2004) for airflow velocity, V, with

$$V = \sqrt{\frac{2D_{\text{H}}\Delta P}{\rho_{\text{in}} f L}}, \tag{4}$$

where D_{H} is the hydraulic diameter of the flow path, f is the Darcy-Weisbach friction factor, and L is the length of the flow path. Combining these two equations, leads to

$$V = \sqrt{\frac{2D_{\text{H}} g h \Delta T}{f L T_{\text{ext}}}}, \tag{5}$$

where one can see that the airflow velocity is predicted to scale with the square root of the temperature difference between outside and cave air. To test the plausibility of chimney effect airflow as the primary mechanism behind the observed airflow in Blowing Springs Cave, airflow velocity is plotted against the temperature difference between inside and outside air, and a square root relationship is fit to the data (Figure 5). Not only is there a strong relationship between temperature difference and cave airflow velocity, but the shape of the relationship is closely matched by a square root function, $V = R\Delta T^{1/2}$, where the best fit value of the resistance factor $R = 0.18$.

There are no known human-sized upper entrances to Blowing Springs Cave. However, we can use knowledge of the cave system to estimate appropriate values of unknown parameters in Equation 5, using $L = 1,000$ m, which is the approximate distance from the entrance to the upstream sump, and $h = 25$ m, which is the approximate elevation difference between the spring entrance and the valleys feeding the cave that are likely to hold upper entrances. Using values of $g = 9.8\,\text{m/s}^2$ and $f = 0.05$, which is a typical value for a rough pipe and high Reynolds Number (Larock et al., 2000), we can estimate that the hydraulic diameter would have to be approximately equal to 1 m in order to produce the observed value of R. Though diameters of the mapped portion of the cave are highly variable (Figure 1), with values reaching up to 5–10 m within larger rooms, a diameter of 1 m is roughly consistent with observed diameters in much of the cave. The untraversable upper portions of the flow paths must also be substantially smaller, because they are too small for a human to enter.

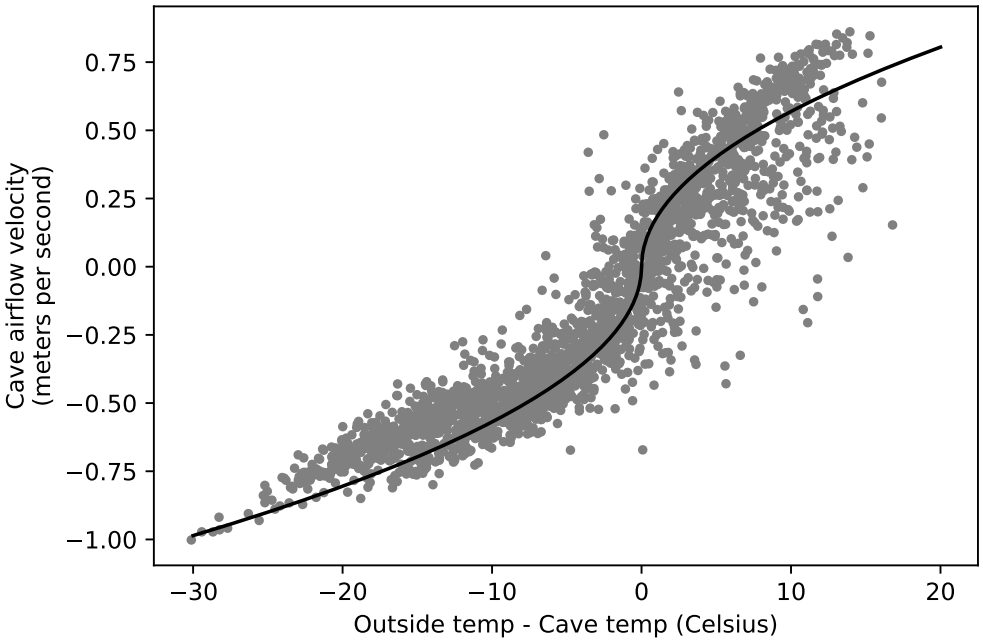

Figure 5: Relationship between airflow velocity and temperature difference between outside air and cave air, with a fitting function $V = R\Delta T^{1/2}$, with the resistance factor set to $R = 0.18$.

To make the link between airflow direction and the chimney effect mechanism explicit in our further discussion, from this point on we will refer to cave airflow direction as either "updraft" or "downdraft" (Figure 6). Updraft occurs during periods when the cave air is less dense than outside air (e.g. winter) and air flows from lower to upper entrances (inward). Downdraft occurs when the cave air is denser than outside air (e.g. summer) and air flows from upper to lower entrances (outward). Because the airflow velocity was measured near a lower entrance, updraft corresponds to inward airflow (negative velocity), and downdraft corresponds to outward airflow (positive velocity). For the study period, the cave exhibited nearly continuous downdraft from June 1 to October 1, and relatively consistent updraft from December 1 to March 1, with occasioanl winter reversals during warm periods. The spring and fall seasons exhibit frequent switching between updraft and downdraft, often diurnally.

4.3. Relationship between airflow velocity and CO_2

The seasonal patterns in cave airflow and CO_2 in the air and water are well aligned (Figure 3). Additionally, there are strong relationships between CO_2 and cave airflow on short timescales (Figure 7). During periods of diurnal airflow reversals, CO_2 in the cave air also shows daily peaks and troughs. When airflow direction switches from downdraft to updraft, cave air CO_2 drops suddenly to concentrations near atmospheric ($\sim 500\,\mathrm{ppm}$), as outside air is quickly brought to the location of the sensor. When airflow switches from updraft to downdraft, cave air CO_2 rises somewhat more slowly, likely as a result of mixing of high and low CO_2 air within the cave atmosphere. Dissolved CO_2 within the cave stream does not respond as rapidly to airflow reversals as the cave air. However, the cave stream CO_2 does have a muted response that has a lag of a few days (Figure 7).

Dissolved and gaseous CO_2 both display statistically significant correlations (p-value$<$0.0001) with airflow velocity when averaged over daily or weekly timescales (Figure 8). Here we quantify correlation using Spearman's rank correlation coefficient because the relationships are non-linear (Helsel and Hirsch, 2002). Correlations are stronger over the weekly timescales than the daily timescales, particularly for dissolved CO_2. The gaseous CO_2 concentrations display a clear threshold near zero airflow velocity (Figure 8), which divides time periods with updraft and downdraft. During periods of updraft, the cave air CO_2 is typically near outside atmospheric concentrations, whereas during downdraft, concentrations substantially increase above

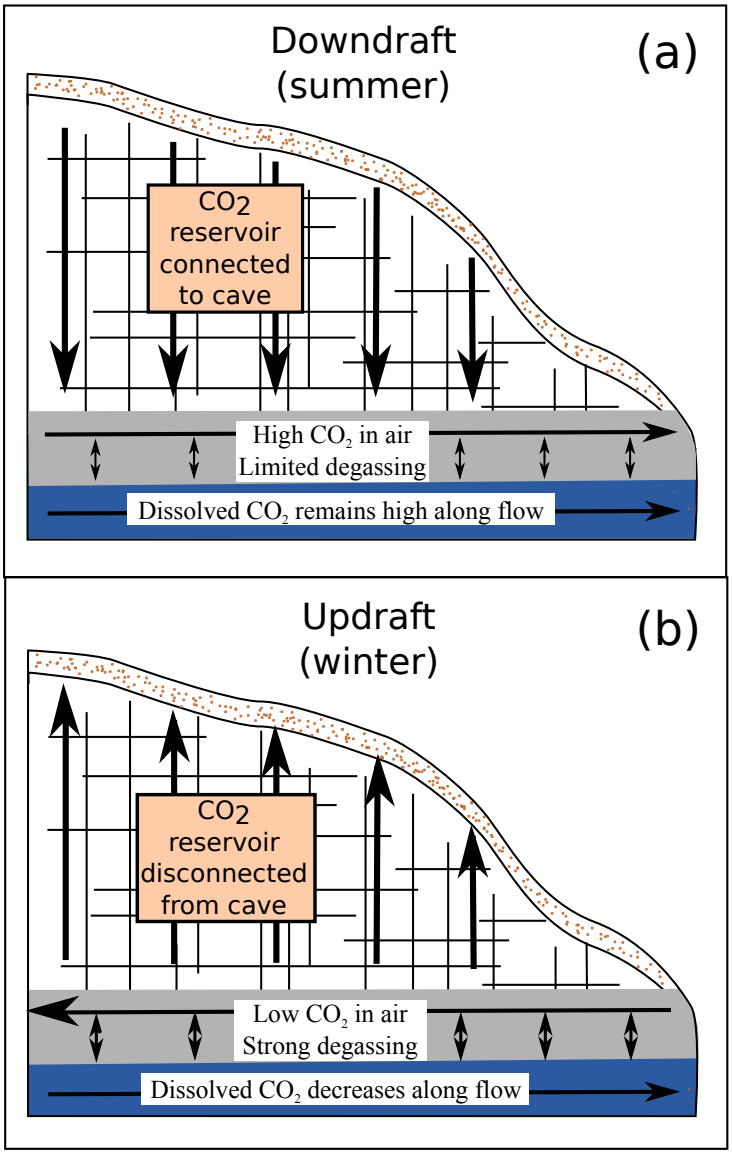

Figure 6: Conceptual model of how ventilation direction impacts dissolution rates in the cave stream: (a) During downdraft (summer conditions), air flows vertically downward through the soil and unsaturated zone, obtaining high CO_2. Cave air pCO_2 is high and therefore degassing of CO_2 from the cave stream is limited. Consequently, dissolved CO_2 and dissolution rates remain high along the main conduit. (b) During updraft (winter conditions), atmospheric air enters the cave through the large lower entrance and then flows upward through the high-CO_2 unsaturated zone. The cave air is disconnected from this high CO_2 zone and strong degassing of CO_2 occurs along the stream, reducing pCO_2 and dissolution rates. During winter storms, vertical flow of water can transport CO_2 through the unsaturated zone and effectively reconnect the cave stream to the CO_2 reservoir.

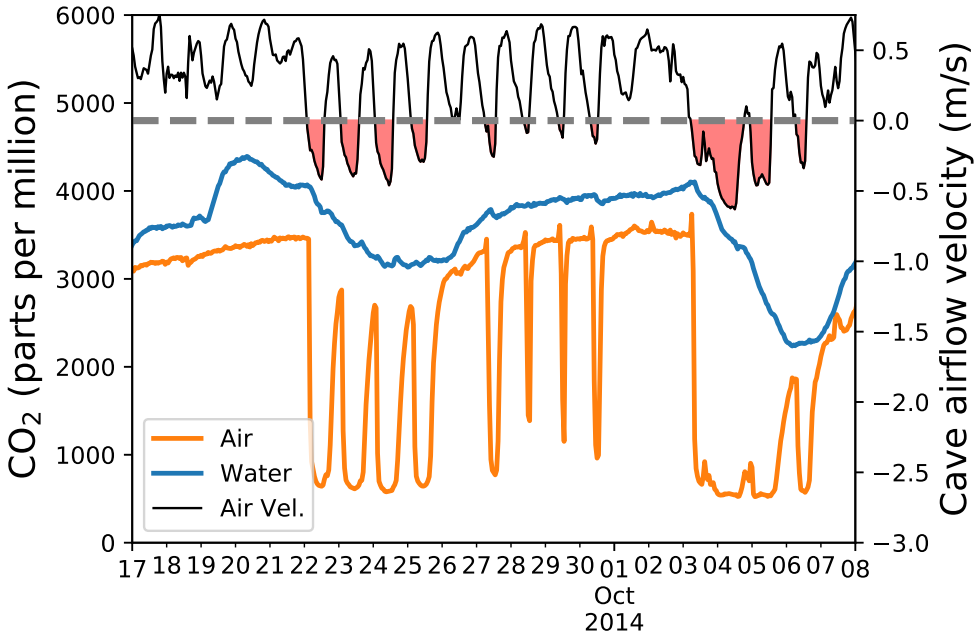

Figure 7: Time series of airflow velocity (top, black), and CO_2 concentrations in air (orange, bottom) and water (blue, middle), where the gray dashed line demarcates zero airflow velocity and the shaded red portions of the curve are periods of updraft (inward airflow). During updraft, gaseous CO_2 concentrations decrease sharply to near atmospheric concentrations. During extended periods of updraft, dissolved CO_2 also decreases. During downdraft CO_2 in the air and water increase.

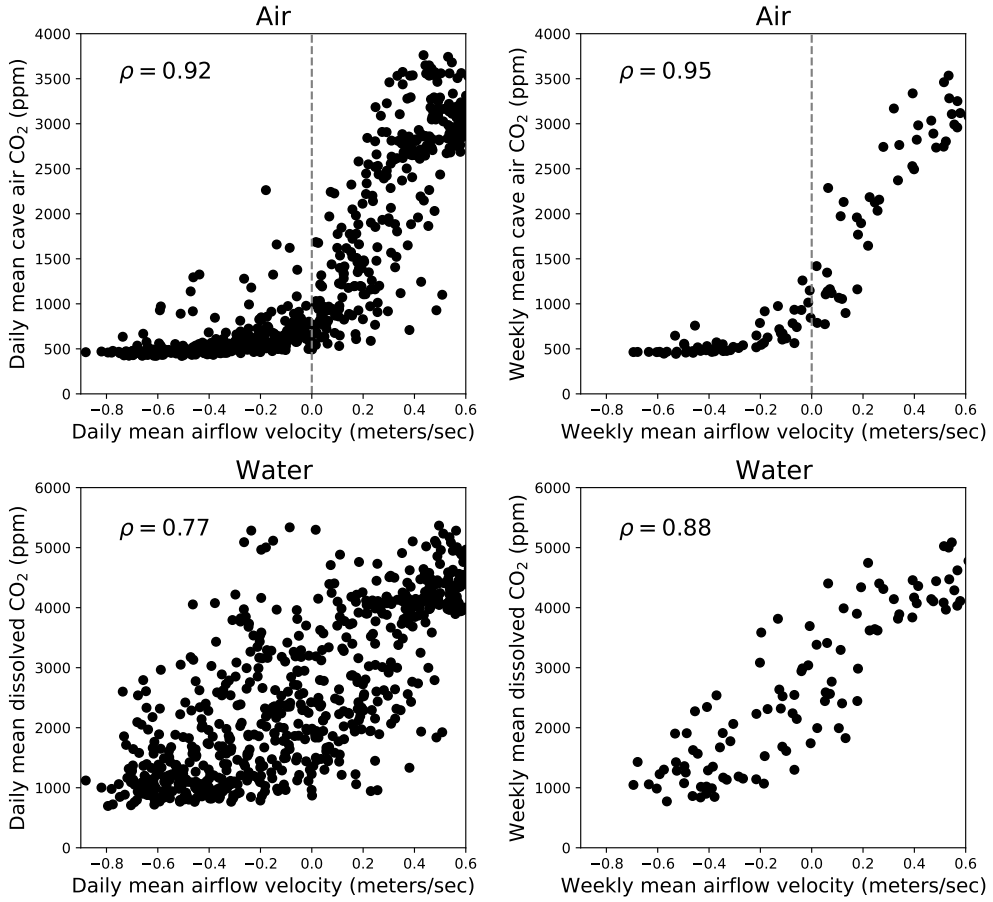

Figure 8: Relationships between airflow velocity and CO_2 concentrations in air and water averaged on daily and weekly timescales. Correlations are quantified using Spearman's rank correlation coefficient ρ. Dashed vertical lines indicate the threshold change in CO_2 concentrations that corresponds to airflow reversals (ppm = parts per million).

atmospheric values. The relationship between dissolved CO_2 and cave airflow does not display a clear threshold at zero cave airflow but still has a clear pattern of lower concentrations during updraft and higher concentrations during downdraft (Figure 8).

4.4. Dissolution rate dynamics in the cave stream

The dissolution rates show a strong seasonal signal that is in-phase with the seasonal CO_2 variation (Figure 9). That is, there are higher rates of dissolution during the summer months, when pCO_2 is also high and the water is undersaturated with respect to calcite. Lower rates of dissolution occur during the winter months (frequently negative PWP rates), when pCO_2 is low and the water is typically supersaturated. The average of this seasonal signal is near calcite saturation (or zero dissolution rate), but the stream spends slightly more time in the undersaturated condition, when dissolution is active. In addition to the seasonal signal, there is clear variability on daily to weekly timescales.

To study the chemical controls on dissolution rate variation, dissolution rates averaged over daily timescales are plotted versus the two primary chemical drivers (Figure 10): dissolved CO_2 and a proxy for dissolved load (SpC). To quantify the correlations between the chemical drivers and dissolution rate, we calculated Spearman's rank correlation coefficients. Both chemical drivers correlate with dissolution rates (p-value$<$0.0001), but CO_2 is more strongly correlated ($\rho = 0.80$) than SpC ($\rho = -0.44$). The cloud of points in the dissolution rate-CO_2 plot (Figure 10a) shows a relatively sharp edge at low dissolution rate. This edge is a result of baseflow conditions, where SpC displays a typical value of about 220 μS/cm.

In addition to direct chemical drivers, dissolution rates vary as a function of external physical controls that produce variations in those chemical drivers. The two most important physical controls on chemical variation at the site are cave airflow velocity and stream discharge. Cave airflow, and particularly its direction, is an important driver of dissolved CO_2 (Figures 6 and 8). Discharge may produce variation in both dissolved load and dissolved CO_2, either through dilution during storm-event runoff or alteration of water sources and flowpaths. Figure 11 shows the relationships between dissolution rate and these two physical drivers over a variety of timescales from daily (a,b), to weekly (c,d), to monthly (e,f). Generally, when airflow velocity is positive (downdraft) and discharge is high, dissolution rate is high.

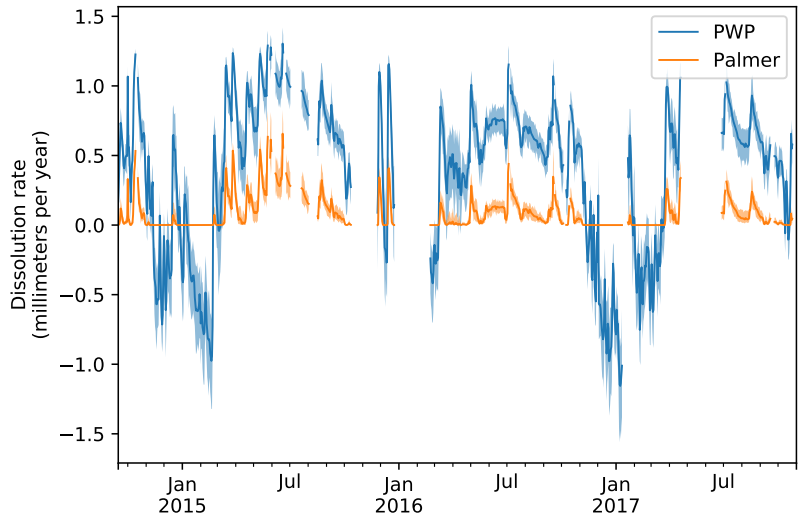

Figure 9: Calcite dissolution rates calculated from pCO_2 and SpC time series, where the blue line depicts rates calculated using the PWP equation (which includes negative values) and the yellow line indicates rates calculated using the Palmer equation. The shaded bands indicate a 90% confidence interval based on the Monte Carlo error propagation. The data indicate a regular seasonal pattern in dissolution rate variability, with undersaturated conditions typical in the summer and supersaturated conditions typical in the winter.

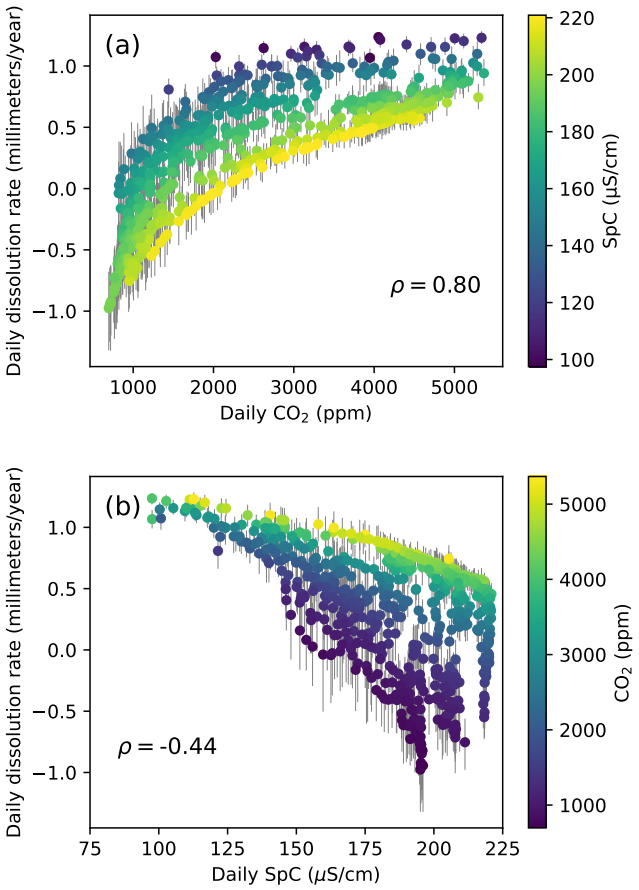

Figure 10: Relationships between daily averaged dissolution rates and (a) pCO_2 (parts per million) or (b) SpC (microsiemens per centimeter), where correlations are quantified using Spearman's rank correlation coefficient, ρ. Error bars depict a 90% confidence interval based on the Monte Carlo error propagation.

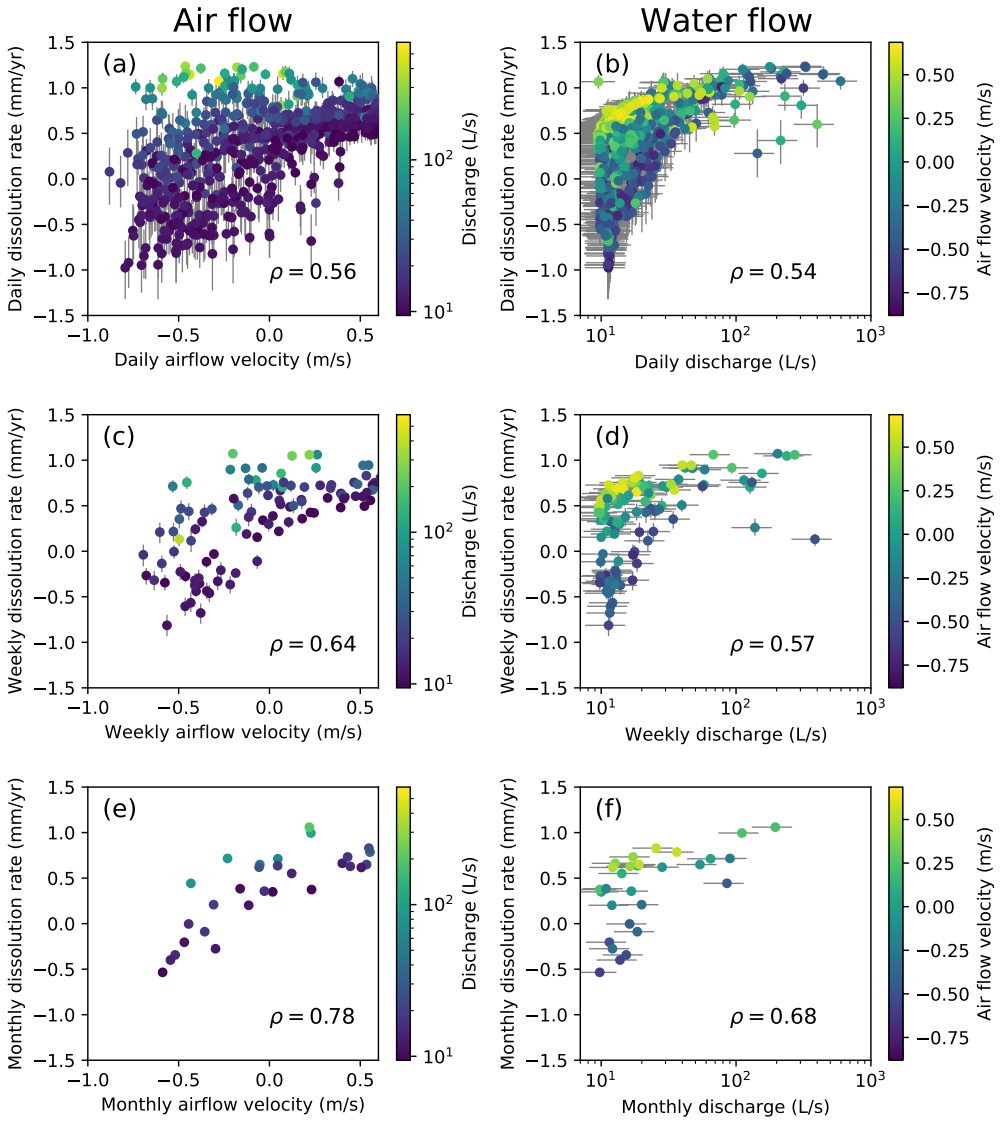

Figure 11: Relationships between dissolution rates and airflow velocity (left column: a,c,e) or stream discharge (right column: b,d,f). Each row represents rates averaged over a different time period, from daily (a,b), to weekly (c,d), to monthly (e,f). Color/shading in the left column indicates discharge and in the right column indicates air flow velocity, and correlations are quantified using Spearman's rank correlation coefficient, ρ. Error bars on dissolution rates depict a 90% confidence interval based on the Monte Carlo error propagation. Error bars on discharge indicate RMSE. Units are: mm/yr = millimeters per year; m/s = meters per second; L/s = liters per second.

At all timescales, cave airflow displays a stronger correlation with dissolution rate than discharge, though at the daily timescale the correlations are effectively the same. The strength of the correlation between airflow velocity and dissolution rate increases with the duration of the averaging. Correlation with discharge is similar for daily and weekly timescales and somewhat higher over the monthly timescale. All correlations have p-values$<$0.0001. Error is known to attenuate correlation (Spearman, 1904), such that large errors will result in bias toward lower correlation. As a result, true correlations are likely modestly higher than the estimates here, particularly for the daily timescale where uncertainties are largest. However, even for the daily timescale, the measured natural variations are substantially larger than the estimated uncertainties.

Since cave airflow velocity emerges as the strongest external driver of dissolution rate variability, and because airflow direction is likely to be the most important factor in determining CO_2 concentrations, we divide the record into days when airflow is on average updraft (winter regime) and downdraft (summer regime). Dissolution rates are higher during periods of downdraft, when the cave air has higher CO_2 (Figure 12). Interestingly, there is also a strong contrast in the variability of dissolution rates during the two airflow regimes, with periods of updraft having much larger variability in rates. This effect is further considered below as we examine how dissolution rates vary during storms.

4.5. Dissolution rate variation during storms

To explore how dissolution rates vary during storms, we first examine relationships between dissolved CO_2 and discharge, because CO_2 is the chemical parameter most strongly correlated with changes in dissolution rate (Figure 10). Since dissolution rates show more variability during upward airflow, one hypothesis might be that airflow direction somehow modulates the variability caused by changes in discharge. As an initial test of this hypothesis, we examine the relationship between daily averaged values of dissolved CO_2 and discharge, separated into groups of downdraft and updraft conditions (Figure 13). Dissolved CO_2 is correlated with discharge during periods of updraft ($\rho = 0.31$, p-value $<$0.0001), whereas there is no statistically significant correlation between dissolved CO_2 and discharge during periods of downdraft airflow ($\rho = 0.05$, p-value $= 0.38$). Again, due to uncertainties in discharge and resulting attenuation of correlation, the real correlations are likely modestly larger than these estimates. However, since the separation in

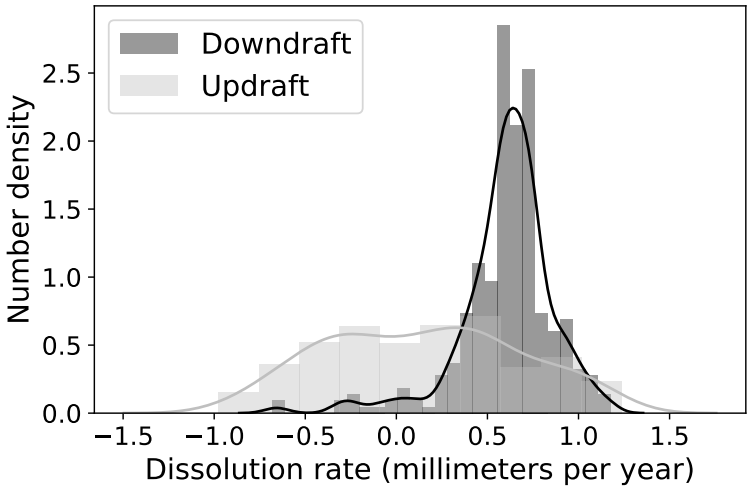

Figure 12: Distribution of dissolution rates under different airflow regimes for daily averaged dissolution rates under both downdraft (dark gray) and updraft (light gray) conditions. During downdraft, dissolution rates are typically high. During updraft, dissolution rates are typically lower; however, they are also much more variable. Kernel density estimates are shown (solid lines) to aid visual distinction of the two overlapping distributions.

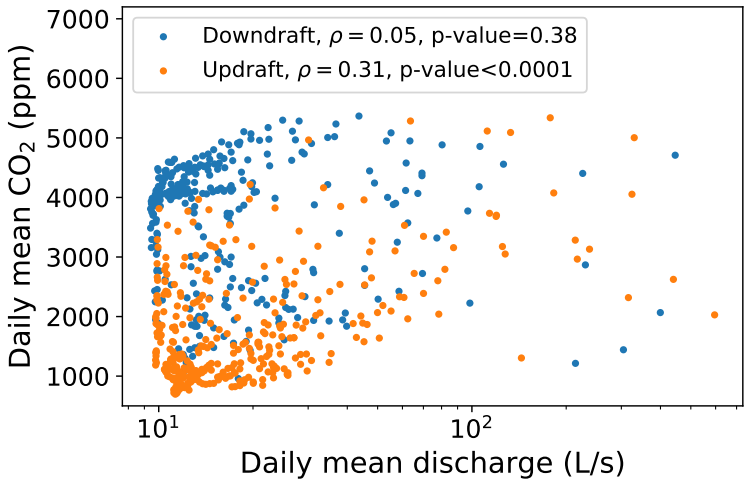

Figure 13: Relationship between discharge and CO_2 under different airflow regimes. Daily averaged values of discharge and CO_2 for periods of either downdraft (blue) or updraft (orange). Spearman's rank correlation coefficients, ρ, and respective p-values indicate that there is a moderate correlation between discharge and CO_2 during periods of updraft airflow but no statistically significant correlation during periods of downdraft airflow. Units are: ppm = parts per million; L/s = liters per second.

ρ and p-values is quite large, we do not expect this to influence the general pattern.

To further examine the possibility that airflow modulates discharge-driven dissolution rate variation during storms, we plot time series of chemistry and estimated dissolution rates during storm events. Two typical examples are shown in Figure 14, one during downdraft (summer) conditions and one during updraft (winter) conditions.

The winter storm produces more variation in dissolved CO_2, which ranges from about 1,000 ppm to 3,500 ppm. Gaseous CO_2 remains low during most of the event because of the dominance of updraft conditions, which bring outside air quickly to the sensor location from the cave entrance. SpC varies from near maximal values, about 220 μS/cm, to 115 μS/cm. Driven by both changes in CO_2 and dissolved load, the dissolution rate changes sharply during the storm, from supersaturated conditions (-0.25 mm/yr) before the storm to highly undersaturated conditions (1.2 mm/yr) near the peak of the event. During the winter storm, estimated discharge ranged from 30 L/s to

330 L/s.

During the summer storm, downdraft conditions prevail, and, consequently, CO_2 concentrations in the air remain relatively high at about 3,000 ppm, except for during two brief periods of airflow reversal that follow the storm. Dissolved CO_2 is already high (4,000 ppm) before the start of the event and peaks about 5,000 ppm during the event. Therefore, there is much less variability of dissolved CO_2 during the summer storm than during the winter storm. SpC decreases during the storm from about 255 μS/cm to about 220 μS/cm, displaying less variability than during the winter storm. Dissolution rate also displays less variability, with rates about 0.5 mm/yr before the storm and 0.8 mm/yr at the peak. During the summer storm, estimated discharge ranged from 8.4 L/s to 80 L/s.

In general, winter and spring (periods of mostly updraft) have higher average values of discharge (Figure 3), as might be expected from lower rates of evapotranspiration during these cooler periods. Therefore, one possibility is that the correlation between airflow direction and dissolution rate variability (Figure 12) is spurious and is actually driven by differences in discharge dynamics during these seasons. Because discharge has a strong negative correlation to dissolved load (Figure 4), storms with greater discharge variation should also have greater variation in dissolved Ca, and this could drive greater variation in dissolution rate.

To explore this possibility we identify all storm events and calculate the range of dissolution rate, the average airflow velocity, and the range of discharge during each storm over the period of record. The beginnings of storms were defined as increases in discharge of at least a factor of two within a period of less than two days. The end of a storm event was defined to be a return to 130% of the pre-storm discharge or one week after the increase in discharge, whichever was shorter. Because most of the chemical variation occurs during the rising limb, the dissolution rate ranges are not particularly sensitive to the criteria for the end of a storm event. However, including these criteria enables treatment of multi-peak events as a single storm. We find that change in dissolution rate within a storm was much more strongly correlated to mean cave air velocity during the storm ($\rho = -0.85$, p-value=0.0004) than it was to the magnitude of the change in discharge ($\rho = 0.23$, p-value=0.45), as is shown in Figure 15 for the storm events for which complete chemical records exist. This suggests that cave airflow direction is an important control on dissolution rate variation during storms, and that storm dissolution rate variability is not primarily driven by dilution.

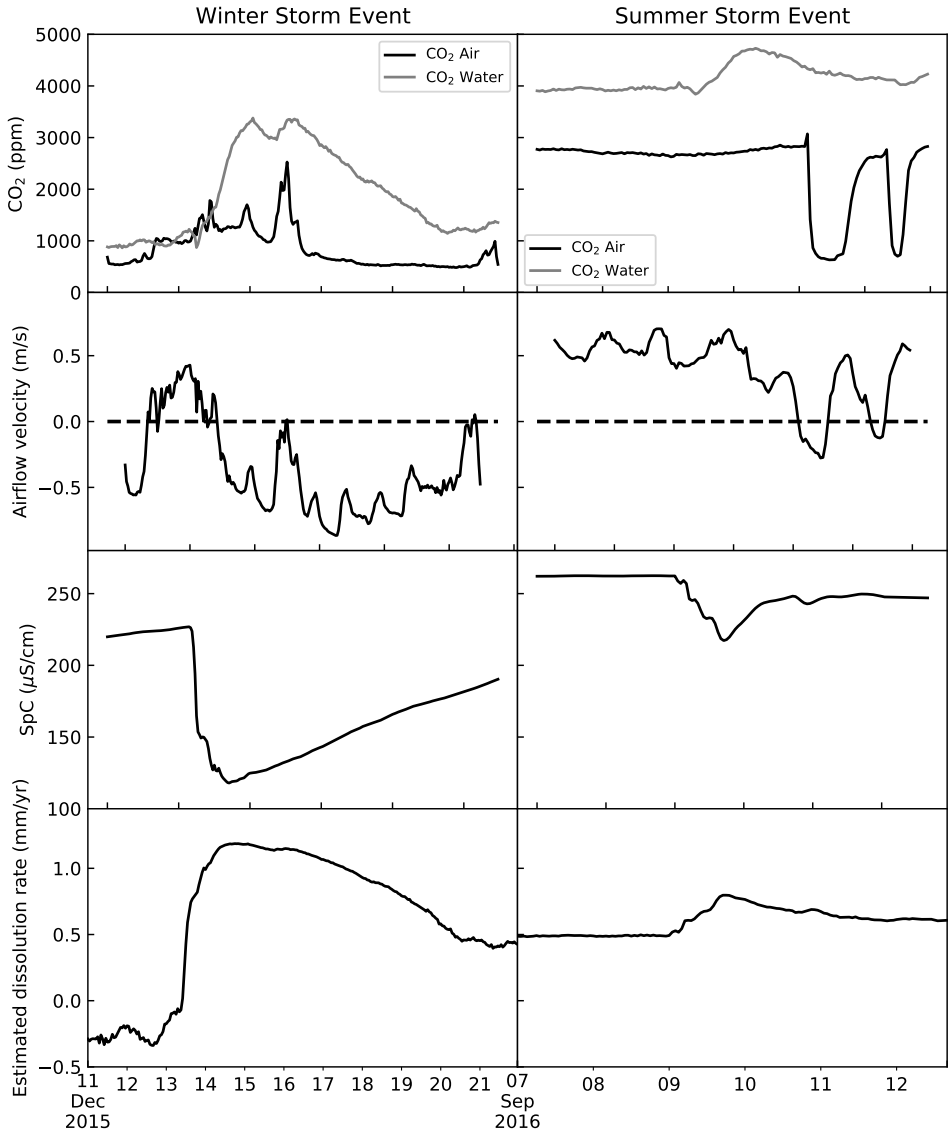

Figure 14: Variability of CO_2, airflow velocity, specific conductance (SpC), and estimated calcite dissolution rate during two example summer and winter storm events. The winter event, when airflow is primarily updraft (negative) exhibits more variation than the summer event in both dissolved CO_2 and SpC, and consequently in dissolution rate. The summer event exhibits low chemical variability. Units are: ppm = parts per million; m/s = meters per second; μS/cm = microsiemens per centimeter; mm/yr = millimeters per year.

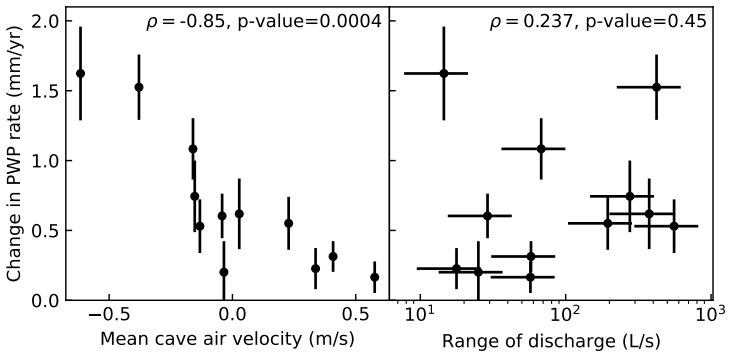

Figure 15: Correlations between storm dissolution rate range and potential controls. Average airflow velocity during a storm event is highly correlated with the range in dissolution rates during the event. The range of discharge within the event is not significantly correlated with the range in dissolution rates. Data are shown for all identified storm events during the study period for which complete chemical records were available. Error bars on dissolution rates depict a 90% confidence interval based on the Monte Carlo error propagation. Error bars on discharge indicate RMSE propagated through the difference used to calculate range.

5. Discussion

5.1. Controls of dissolution rate variability

The concept of the magnitude and frequency of erosional forces is central to understanding how temporal variations in the rates of geomorphic processes influence the long-term rates of landscape evolution and the morphologies that develop (Wolman and Miller, 1960). This concept is most frequently applied in fluvial systems, where frequency relates to the recurrence interval of streamflows of different magnitude. However, magnitude and frequency have also been discussed in the context of weathering processes, such as chemical solution (Goudie and Viles, 1999).

A variety of studies have quantified variation in rates of chemical geomorphic work at the basin scale by examining the rate of solute export as a function of river streamflow (Wolman and Miller, 1960; Gunn, 1982; Schmidt, 1985). However, quantifying magnitude and frequency within the context of weathering presents some challenges, and, particularly one must be clear as to the specific process that one is attempting to quantify (Goudie and Viles, 1999). Calculating chemical weathering rates using river solutes provides a

quantification of the magnitude and frequency attributes of solute export from a basin. However, since solutes are stored within the basin for some unknown time, these rates are removed from the rates of actual detachment of the ions from mineral surfaces. For example, Covington et al. (2015) show that in-stream calcite dissolution rates may be orders of magnitude higher than basin-wide denudation rates derived from basin solute export. One can imagine, similarly, that the time variability of rates of dissolution on karst landscape surfaces might be quite different than the time variability in basin-wide solute export rates.

Relatively few studies have attempted to quantify the time-variation of calcite dissolution rates within karst streams or caves, or to understand the controls of this variability (Groves and Meiman, 2005; Palmer, 2007b; Galdenzi, 2012; Covington et al., 2015; Covington and Vaughn, 2019). The central goal of this study was to examine variability in dissolution rates within a specific cave stream and to develop a mechanistic understanding of the controls on that variability.

As in previous studies (Groves and Meiman, 2005; Covington et al., 2015; Covington and Vaughn, 2019), we find that the strongest chemical driver of variation in dissolution rates is variation in dissolved CO_2, which shows much stronger correlation with dissolution rate at our site than does dissolved load (Figure 10). In turn, dissolved CO_2 displays a strong seasonal pattern. This seasonal pattern is strongly correlated with seasonal changes in the cave air CO_2 that are driven by the direction of cave airflow (Figures 3a-b and 8), which is ultimately controlled by the temperature difference between cave air and outside air (Equation 5). A conceptual sketch of the interactions between these processes is shown in Figure 6. Review of time series data over shorter timescales (days to weeks) provides even stronger evidence for a mechanistic connection between cave airflow and dissolved CO_2, where switches in airflow direction strongly perturb CO_2 concentrations in the cave atmosphere, and the dissolved CO_2 in the cave stream responds in a lagged and muted fashion, decreasing during periods of low cave air CO_2 and increasing during periods of high cave air CO_2 (Figure 7).

Review of the entire dataset shows that, perhaps surprisingly, dissolution rate is more strongly correlated with cave airflow velocity than with discharge (Figure 11). The difference in the correlation strength increases moving from daily to monthly timescales, suggesting that cave airflow is most important in impacting the seasonal pattern though still has a strong impact on the timescales of storms. Similar observations have been made on the impact of

cave ventilation on the saturation state of drip water and resulting seasonal biases within speleothem records (Spötl et al., 2005; Banner et al., 2007; Wong et al., 2011), and ventilation has also previously been argued to impact spatial or temporal changes in cave stream dissolved CO_2 or dissolved load (Troester and White, 1984; Jeannin et al., 2017). Gulley et al. (2014) also found that seasonal cave ventilation patterns can explain seasonal changes to dissolved load and dissolved CO_2 within a water table cave in Florida. Therefore, the patterns observed here cohere with previous studies, though our data provide much higher time resolution to examine the connections between ventilation and cave stream saturation state in more detail.

Though the time series data suggest that cave airflow direction is an important control of the seasonal oscillation of dissolved CO_2, there may be additional drivers. Specifically, CO_2 production in the soil through microbial decay and root respiration is known to vary with surface temperature and solar radiation (Hibbard et al., 2005; Lloyd and Taylor, 1994). At a nearby site with a similar hydrogeological setting, Covington and Vaughn (2019) observed a strong seasonal signal (range $\approx$ 20,000 ppm) in dissolved CO_2 at Langle Spring, Arkansas, which is thought to drain an unventilated portion of the karst aquifer. They hypothesized that this signal derived from seasonal changes in subsurface CO_2 production. It is uncertain how much of the seasonal signal in dissolved CO_2 at Blowing Springs might also be a function of changes in the rate of CO_2 production.

In contrast to the seasonal respiration-driven pattern, some karst aquifers that exhibit higher pCO_2 at depth than in the soil have very little seasonal CO_2 variation at depth (Atkinson, 1977a). A prior study at Blowing Springs Cave measured soil CO_2 concentrations, with summer values frequently being above what we observe in the cave stream and winter values frequently being below (Knierim et al., 2017). Additionally, the study used stable carbon isotopes to quantify the mixture of atmospheric CO_2 versus unsaturated zone CO_2 (produced via respiration/decomposition) in the cave atmosphere. Knierim et al. (2017) found that the proportion varied seasonally and, additionally, that there were different mixing lines for each season, highlighting seasonally variable unsaturated zone CO_2 sources. At the least, these observations suggest that there is some storage of CO_2 in the unsaturated zone that might reduce seasonal variation in the cave. The few available on-site measurements of dissolved CO_2 at the upstream sump in Blowing Springs Cave indicate a range of approximately 1,500 ppm between summer and winter measurements (Young, 2018), in contrast to the range of approximately

5,000 ppm that we observe near the downstream end of the cave. However, it is also unclear how much ventilation might occur within the portion of the aquifer that is upstream of the sump. Therefore, whereas there is a clear impact of cave ventilation on the annual CO_2 cycle, there may also be a seasonal signal driven by production. The magnitude of that production signal is uncertain.

The mechanistic link between cave airflow direction and dissolved CO_2 in the stream is generated because the primary CO_2 source for the cave air can either be upwind or downwind of the main cave stream (Figure 6). The primary source of CO_2 to the cave atmosphere is a CO_2 reservoir within the soil and unsaturated zone above the cave. During periods of downdraft (summer regime) ventilation brings gases from this reservoir into the cave, maintaining a high pCO_2 within the cave air that limits degassing of CO_2 from the cave stream (Figure 6a). During periods of updraft (winter regime) ventilation brings fresh outside air into the cave, reducing the pCO_2 of the cave air and enhancing degassing of CO_2 from the stream (Figure 6b). Though the cave has strong ventilation during both summer and winter conditions, the restricted nature of the airflow pathways through the unsaturated zone must produce a sufficiently high surface area to volume ratio that air transiting this zone obtains a high pCO_2.

5.2. Dissolution rate variability during storms and the role of airflow

Whereas storms play a secondary role in driving variability in dissolution rates, there are still statistically significant correlations (alpha=0.05) between discharge and dissolution rate (Figure 11b). We can observe these variations clearly on the basis of individual storms, and see that they are driven by a combination of dilution and increasing dissolved CO_2 (Figure 14). Interestingly, airflow direction also appears to modulate the dissolution rate variability within storms, with greater storm variability during updraft conditions. This is supported by at least three observations:

1. Variation in dissolution rates is much greater during updraft than downdraft (Figure 12);
2. Dissolved CO_2 is positively correlated with discharge during updraft but not during downdraft (Figure 13);
3. Dissolution rate range during individual storms is correlated to the airflow velocity but not to the range of discharge during the storm (Figure 15).

It is perhaps counterintuitive that cave airflow direction should have any importance for dissolution rate variation during storms. However, the observed pattern can be explained using an existing conceptual model for unsaturated zone CO_2 within karst (Mattey et al., 2016) and a basic mathematical framework for transport of CO_2 within the karst unsaturated zone (Covington, 2016). Mattey et al. (2016) argue, based on eight years of field measurements at the Rock of Gibraltar and other observations of deep CO_2 within karst systems (Atkinson, 1977a; Wood, 1985; Wood and Petraitis, 1984), that karst unsaturated zones contain a body of "ground air," which is a reservoir of CO_2 produced by the microbial decay of organic matter that has infiltrated to depth. Cave air is considered to be a mixture of surface air with ground air, where the percentages depend largely on the outside temperature and the resulting direction of air circulation through the unsaturated zone.

Other work has suggested that the CO_2 in cave air is often associated with root respiration of the deepest rooting plants (Breecker et al., 2012), again suggesting production at depth. At Blowing Springs Cave, the carbon isotope ratios of CO_2 are consistent with soil/root respiration (Knierim et al., 2017) (with summer values around -21‰), so it is unclear whether the source of deep unsaturated zone CO_2 might be particulate organic matter or from root respiration. However, to explain the observations, we hypothesize that there is a substantial volume of CO_2 stored at depth in the unsaturated zone.

During winter (periods of cave updraft), storms bring water that is charged with CO_2, frequently 2,000–4,000 ppm. These concentrations are substantially higher than typically observed in soil at the site during fall/winter (1,500 ppm) in a prior study (Knierim et al., 2017). This observation supports the conception of a reservoir of high pCO_2 within the unsaturated zone (Atkinson, 1977a; Mattey et al., 2016). Additionally, a simple model of CO_2 transport within a vertical fracture suggests that vertical flow of water through karst fractures can efficiently redistribute CO_2 within the subsurface, pushing it to greater depth (Covington, 2016). Observations of hysteresis between discharge and dissolved CO_2, with higher CO_2 during the recession, have also been interpreted as indicating that later arriving diffuse recharge water can transport soil and unsaturated zone CO_2 into karst conduits (Vesper and White, 2004). Therefore, it is physically plausible that vertical flow of water through the unsaturated zone during a storm could effectively transport a pulse of CO_2 to the water table.

Downward transport of CO_2 during winter storms produces variation in

the cave stream because the winter airflow regime has disconnected the cave stream from the CO_2 source (Figure 6b), reduced the pCO_2 of the cave stream, and the pulse of high CO_2 has a large effect. Conversely, in the summer airflow regime (downdraft) the cave air is already in contact with the ground air (Figure 6a), because the air is entering the cave via the soil and unsaturated zone. Therefore, degassing is reduced and the cave stream is maintained at high pCO_2. Consequently, summer storms produce much less variation in CO_2 within the cave stream and therefore less variation in dissolution rate. This conceptual model is also supported by previous work at Blowing Springs Cave where isotopic disequilibrium between dissolved inorganic carbon (DIC) in the cave stream and CO_2 in the cave air was greater during winter periods, when the cave stream is disconnected from the CO_2 source, but approached equilibrium during summer, when cave air CO_2 was higher (Knierim et al., 2017).

5.3. Dissolution rate variation in the context of similar studies

Since discharge is not the primary driver of variation in dissolution rates at the study site, normal concepts of magnitude and frequency break down, as they are based on flood recurrence intervals. To estimate rates of geomorphic work in the cave stream, we are better off asking, "Which way is it blowing?" rather than, "How much is it flowing?" However, this pattern is seemingly not a universal one, and it is worth putting into the context of the limited set of other studies of dissolution rate variation in karst conduits.

First we compare against the nearby study of Langle and Copperhead Springs (Covington and Vaughn, 2019), located in the same limestone layer and climate setting as Blowing Springs Cave. These two springs compose a karst underflow-overflow system, where Langle Spring is completely phreatic and carries most of the flow at low discharge. Langle and Copperhead Spring both exhibit strong seasonal CO_2 variation that is the strongest control on dissolution rate. Data suggest that Langle drains a relatively small phreatic conduit, which has no ability to ventilate. Langle Spring has the highest variation in CO_2 concentration of any of the available studies of dissolution rates within karst conduits, with summer values that exceed 20,000 ppm and winter values about 3,000 ppm. One potential reason for the higher CO_2 concentrations and strong production-related signal is that land use in the spring recharge zone is predominantly pasture, and grasslands have higher CO_2 production rates than forested areas (Smith and Johnson, 2004; Knierim et al., 2015a, 2017). Copperhead Spring has peak values in early summer

about 15,000 ppm and then late summer values about 5,000–6,000 ppm, which are similar to peak summer values at Blowing Spring. The sudden decrease in CO_2 at Copperhead Spring in the early summer coincides with a discharge threshold. Below this threshold, the cave system feeding this spring begins to ventilate, and CO_2 decreases dramatically as a result of the onset of ventilation (Covington and Vaughn, 2019). Therefore, if we want to estimate dissolution rates at Langle Spring, we need to consider variability in soil CO_2 production, and might ask ourselves, "Is it growing?" Whereas, at Copperhead Spring, which is intermittently ventilated, it is more important to ask, "Is it blowing?"

In the two other cave streams where dissolution rate or saturation state has been quantified as a function of discharge (Groves and Meiman, 2005) or recurrence interval (Palmer, 2007b), the cave water was supersaturated during most of the study period, with only short periods of active dissolution occurring at high flow. Groves and Meiman (2005) studied the Logsdon River in Mammoth Cave, Kentucky, and Palmer (2007b) studied McFail's Cave, New York. Both studies found that the majority of the dissolution occurs in the top 5% flow regime. Therefore, these sites fall more into the standard magnitude and frequency framework, where active dissolution is driven by high flow events.

One reason for the tendency toward supersaturation at these two sites may be that they are more highly ventilated than any of the other study sites. Mammoth Cave is the longest cave in the world (Gunn, 2004), has many entrances, and is, consequently, well-ventilated. This high density of entrances may produce relatively low CO_2 concentrations in the cave air during all seasons. Therefore, water flows through the soil and unsaturated zone dissolving calcite under relatively high pCO_2 conditions, then it enters the cave stream, is brought to much lower pCO_2, and becomes supersaturated. Storm events may in part increase dissolution rates by reducing ventilation when portions of the system flood to the ceiling. During the largest flood event in the study, Logsdon River remained under pipefull flow conditions for 114 hours (Groves and Meiman, 2005). An additional factor that may create variability with discharge is the nature of recharge to the system. Approximately 40% of the recharge to Logsdon River is allogenic (from streams flowing off of sandstone caprock). It is plausible that flow from non-carbonates, and changes to the percentage of that flow during floods, could increase the sensitivity of dissolution rates to discharge (Atkinson, 1977b; Scanlon and Thrailkill, 1987; Worthington et al., 1992). Palmer (2007b) also describes McFail's Cave as

"well-aerated," and suggests that the cave stream is supersaturated because of ventilation and degassing of CO_2. Therefore, it is plausible that episodic storm-driven dissolution is a common pattern within highly ventilated karst conduit systems, which typically have low concentrations of dissolved CO_2.

5.4. The role of ventilation over the history of cave evolution

Taken within the context of prior studies (Groves and Meiman, 2005; Palmer, 2007b; Covington and Vaughn, 2019), the data presented here elucidate how ventilation may drive changes in dissolution rates within karst conduits as they evolve. The observed behaviors can be arranged on an axis of increasing ventilation (Figure 16). Except during periods of base-level aggradation, karst systems will also tend to evolve along this axis over time, from no ventilation at the beginning toward highly ventilated as they mature.

During the first stage of karst conduit evolution, the pre-breakthrough stage (Figure 16a), the penetration length of undersaturated water is less than the length of the incipient conduit (Dreybrodt, 1996; Covington et al., 2012). Consequently, calcite dissolution under closed-system conditions within the flowpath leads to the consumption of CO_2, which greatly reduces dissolution rates at depth.

Once breakthrough occurs, and the penetration length exceeds the flowpath length, then water can traverse the conduit without substantially reduced pCO_2 despite the closed-system conditions (Covington and Vaughn, 2019). This is the stage that we observe at Langle Spring (Figure 16b), the pattern that we refer to as, "Is it growing?" This stage shows the highest average dissolution rates among the study sites compared here. These high rates are maintained because the water is at high pCO_2 and has no means of degassing that CO_2. At Langle Spring, there is a strong seasonal signal driven by CO_2 production. However, some karst springs have very low annual variation in pCO_2 (Atkinson, 1977a), so this seasonal pattern is not universal. Why some karst systems have a strong production-related signal, and some do not, remains an open question.

The third stage, "Is it blowing?" represents the onset of intermittent ventilation (Figure 16c), where the karst system is intermittently ventilated. For Copperhead Spring, this switch is driven by changes in water level. The temporal changes in dissolution rate at this site show a seasonal signal, but superimposed on that seasonal signal is a strong switching behavior where periods of ventilation dramatically reduce the dissolution rates.

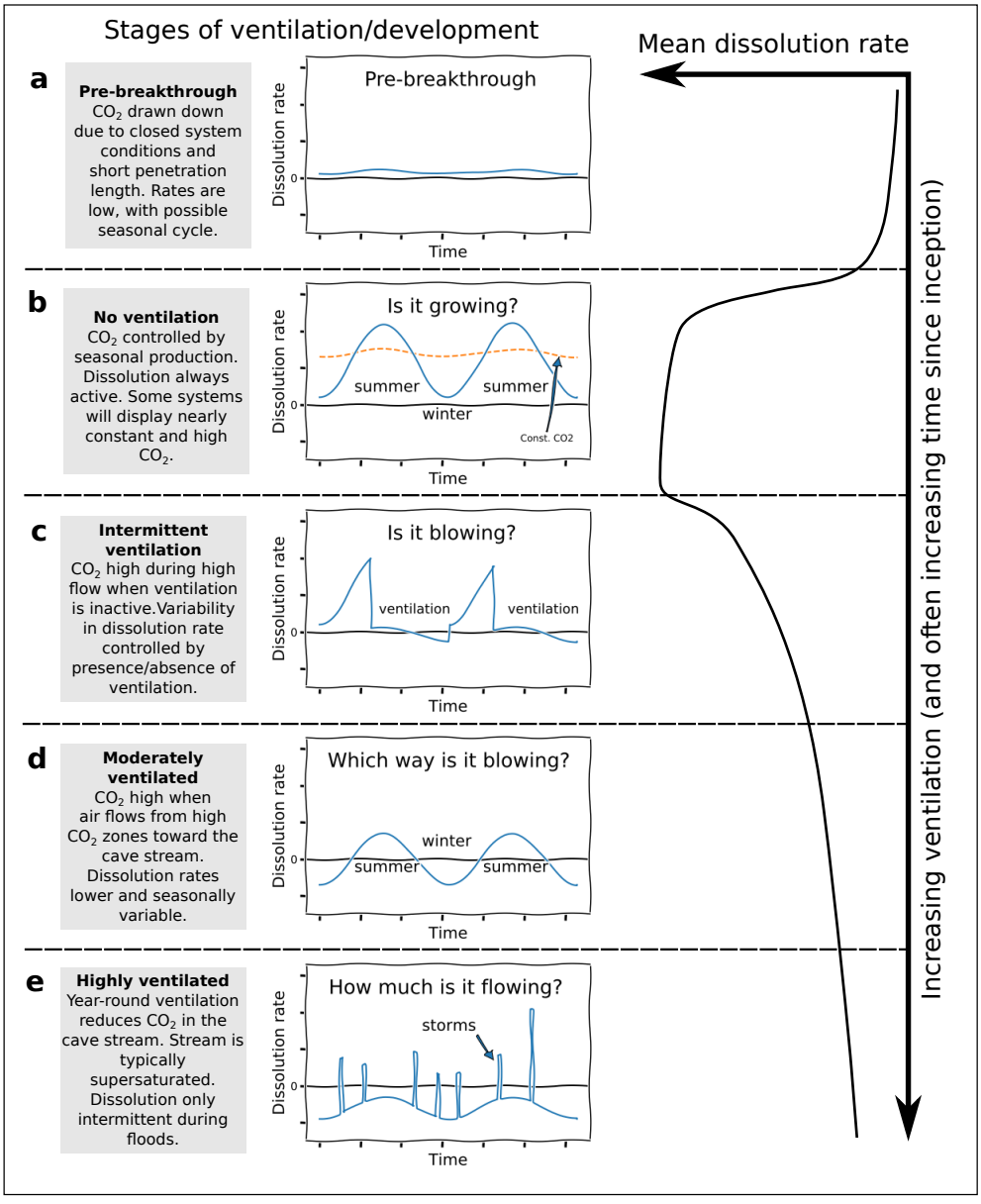

Figure 16: Patterns of observed dissolution rate variation from this and other studies and how they relate to ventilation strength and resulting CO_2 dynamics. Except during periods of base-level aggradation, caves will typically evolve toward being more ventilated over time.

The fourth stage, moderately ventilated, is observed at Blowing Springs Cave (Figure 16d). During this stage the conduit undergoes continuous ventilation. However, the direction of airflow strongly impacts dissolution rates. We ask, "Which way is it blowing?" The seasonal ventilation patterns that are driven by chimney effect airflow create a seasonal pattern in dissolution rate as the CO_2 source switches between being upwind and downwind of the cave stream. The seasonal pattern is more muted than in the previous two stages, and the average dissolution rates are lower.

At Blowing Springs, we see secondary variability driven by storms, which typically increase dissolution rates. However, even this storm variation is modulated by airflow direction. To create the moderately ventilated pattern of dissolution rate variability, the CO_2 of air passing through the zone of CO_2 sources must be strongly influenced by those sources. The exact physical requirements for this influence are unclear. However, the rate and spatial distributions of CO_2 production may be important. Furthermore, the air pathways must have a sufficiently high surface area to volume ratio in order to create effective exchange of CO_2. This may be more likely if airflow is divided between many smaller pathways. Clearly, if an air pathway is too open, then it will rapidly bring in outside air that reduces the pCO_2.

The final stage is a highly ventilated cave (Figure 16e) and is illustrated by prior studies at Mammoth Cave and McFail's Cave. Here, we return to the more standard framework for considering variation in geomorphic work within a stream, "How much is it flowing?" Within these systems, ventilation is sufficiently strong that the stream is normally in supersaturated conditions. There may still be a seasonal variation in CO_2 (Groves and Meiman, 2005), but dissolution primarily occurs during short-term high-flow events. This variation may be driven by dilution, particularly in the case of allogenic recharge, and may also be driven by temporary shutoff or reduction of ventilation as many conduits transition into full pipe conditions during a flood. Pulses of CO_2 brought through the unsaturated zone by water may also impact cave stream CO_2, as observed at Blowing Springs Cave.

After initial conduit breakthrough (2nd stage, Figure 16), the overall pattern is one of increasing ventilation and, as a result, decreasing pCO_2 and decreasing dissolution rates (Palmer, 2007b). Therefore, we might expect that chemical erosion rates within cave streams gradually reduce over the history of evolution, except perhaps during periods of base level rise, where more conduits would become flooded. This trend toward reduced chemical erosion rates over time also has implications for the importance of mechan-

ical erosion within cave streams. Since instantaneous chemical erosion rates are limited to relatively low magnitudes in comparison to mechanical erosion (Covington et al., 2015), this result suggests that mechanical erosion processes should become much more important once caves are well-ventilated. For the well-ventilated end member, only intermittent dissolution is observed during floods. These same flood events are likely to overcome thresholds for transport of sediment and consequent mechanical erosion. Using the tortoise and the hare analogy (Simms, 2004), chemical erosion processes are most effective when they occur nearly continuously (tortoise). If chemical erosion processes become intermittent, mechanical erosion is likely to dominate.

While we have sketched a broad hypothesis about how ventilation controls the rate of calcite dissolution within karst conduits, and how that role might evolve as a karst system matures, the observed patterns come from a relatively limited set of karst systems that are far from spanning the full range of climatic and geological settings of karst. Therefore, there are likely other potential controls on dissolution rate variability and perhaps other ways in which ventilation interacts with CO_2 dynamics. The conceptualization in Figure 16 is relatively simplistic, and it seems likely to grow in complexity as further sites are studied and more dimensions of the problem are understood. Importantly, all of the sites discussed are dominated by autogenic recharge. It seems plausible that sites dominated by allogenic recharge will display somewhat different dynamics. For example, ventilation may not bring water to a supersaturated state, because dissolved load is always sufficiently low. Dilution may be more important. However, patterns of CO_2 production and degassing have also been shown to control spatial patterns of dissolution within allogenically recharged systems (Covington et al., 2013).

Here we have categorized each study site into a single pattern/stage of Figure 16, but most karst systems will contain a range of ventilation conditions within them. Therefore, the presented stages may also represent spatial contrasts in dissolution rate dynamics within different portions of a karst system that have different ventilation strengths. Processes such as CO_2 production, ventilation, and gas exchange are currently absent from numerical models of speleogenesis. Developing and exploring mathematical models for these processes would aid future understanding of the long-term interactions among ventilation, CO_2 dynamics, and calcite dissolution and how they influence the rates and patterns of cave development.

6. Conclusions

We collected time series data from a stream cave in Arkansas to study the temporal variation in calcite dissolution rates and the factors that drive them. Ventilation of the cave atmosphere is driven by external temperature changes through the process of chimney effect airflow. The direction of air flow is the primary control on gaseous CO_2 within the cave atmosphere, with low CO_2 during periods with updraft, when the cave is effectively ventilated by outside air, and high CO_2 during periods of downdraft, when outside air flows through a zone of high CO_2 before entering the main cave passage. In turn, dissolved CO_2 in the cave stream is strongly impacted by the concentration of CO_2 in the cave atmosphere, generating a seasonal variation in dissolved CO_2 that emerges as the primary driver of dissolution rate variability within the cave stream. Dissolution rate is more strongly correlated with cave airflow direction than it is with discharge, indicating that the standard framework of geomorphic work partitioned by flood stage is inappropriate for this site. We also find that the variations of dissolution rates during individual storm events are modulated by airflow direction, with more variation occurring during updraft (winter) conditions. We compare the results from this study with prior studies of dissolution rate variability within karst systems and propose a preliminary framework to explain the different observed patterns of dissolution rate variation along an axis of increasing cave ventilation. We suggest that the onset of ventilation reduces the rates of chemical erosion within karst systems, and that as karst systems mature they will generally evolve toward greater ventilation and lower dissolution rates. This effect may accentuate the importance of mechanical erosion during the later stages of cave evolution.

Acknowledgments

We thank Joshua Blackstock, Alex Breeding, Brandon Conlon, Max Cooper, Katarina Kosič, Joe Myre, Matija Perne, and Evan Thaler for assistance in the field. We thank the Bella Vista Property Owners Association for access to Blowing Springs Cave. This material is based upon work supported by the National Science Foundation under Grant No. EAR 1226903. Any opinions, findings, and conclusions or recommendations expressed in this material are those of the authors and do not necessarily reflect the views of the NSF. Any use of trade, firm, or product names is for descriptive purposes only and does not imply endorsement by the U.S. Government.

Data Availability

The data used in this manuscript and the python code that was used to analyze the data and create the figures are provided in a Github repository that is archived on Zenodo: `https://doi.org/10.5281/zenodo.3839802`.

References

Adamski, J.C., Petersen, J.C., Freiwald, D.A., Davis, J.V., 1995. Environmental and hydrologic setting of the Ozark Plateaus study unit, Arkansas, Kansas, Missouri, and Oklahoma. U.S. Geological Survey Water-Resources Investigations Report 94-4022, 69 p.

Atkinson, T., 1977a. Carbon dioxide in the atmosphere of the unsaturated zone an important control of groundwater hardness in limestones. Journal of Hydrology 35, 111–123.

Atkinson, T., 1977b. Diffuse flow and conduit flow in limestone terrain in the Mendip Hills, Somerset (Great Britain). Journal of Hydrology 35, 93–110.

Badino, G., 2010. Underground meteorology - What's the weather underground? Podzemna meteorologija: Kakšno je vreme v podzemlju?. Acta Carsologica 39, 427–448.

Banner, J.L., Guilfoyle, A., James, E.W., Stern, L.A., Musgrove, M., 2007. Seasonal Variations in Modern Speleothem Calcite Growth in Central Texas, U.S.A. Journal of Sedimentary Research 77, 615–622.

Blackstock, J.M., Covington, M.D., Perne, M., Myre, J.M., 2019. Monitoring Atmospheric, Soil, and Dissolved CO2 Using a Low-Cost, Arduino Monitoring Platform (CO2-LAMP): Theory, Fabrication, and Operation. Frontiers in Earth Science 7.

Bonacci, O., 2001. Analysis of the maximum discharge of karst springs. Hydrogeology Journal 9, 328–338.

Brahana, J.V., 2011. Ten Relevant Karst Hydrogeologic Insights Gained from 15 Years of In Situ Field Studies at the Savoy Experimental Watershed, in: Kuniansky, E. (Ed.), U.S. Geological Survey Karst Interest Group Proceedings, Fayetteville, Arkansas, April 26-29, 2011, U.S. Geological Survey Scientific Investigations Report 2011-5031. pp. 132–141.

905 Breecker, D.O., Payne, A.E., Quade, J., Banner, J.L., Ball, C.E., Meyer,
906 K.W., Cowan, B.D., 2012. The sources and sinks of CO2 in caves under
907 mixed woodland and grassland vegetation. Geochimica et Cosmochimica
908 Acta 96, 230–246.

909 Covington, M., Perne, M., 2015. Consider a cylindrical cave: A physicist's
910 view of cave and karst science. Acta Carsologica 44, 363–380.

911 Covington, M., Vaughn, K., 2019. Carbon dioxide and dissolution rate dy-
912 namics within a karst underflow-overflow system, Savoy Experimental Wa-
913 tershed, Arkansas, USA. Chemical Geology 527, 118689.

914 Covington, M.D., 2007. Map of Blowing Springs Cave, Bella Vista, Arkansas.
915 Boston Mountain Grotto, Fayetteville, AR.

916 Covington, M.D., 2016. The importance of advection for CO2 dynamics
917 in the karst critical zone: An approach from dimensional analysis, in:
918 Geological Society of America Special Papers: Caves and Karst Across
919 Time. Geological Society of America. volume 516, pp. 113–127.

920 Covington, M.D., Gulley, J.D., Gabrovšek, F., 2015. Natural variations in
921 calcite dissolution rates in streams: controls, implications, and open ques-
922 tions. Geophysical Research Letters 42, 2836–2843.

923 Covington, M.D., Luhmann, A.J., Wicks, C.M., Saar, M.O., 2012. Process
924 length scales and longitudinal damping in karst conduits. Journal of Geo-
925 physical Research 117, 1–19.

926 Covington, M.D., Prelovšek, M., Gabrovšek, F., 2013. Influence of CO2
927 dynamics on the longitudinal variation of incision rates in soluble bedrock
928 channels: Feedback mechanisms. Geomorphology 186, 85–95.

929 Dreybrodt, W., 1996. Principles of early development of karst conduits under
930 natural and man-made conditions revealed by mathematical analysis of
931 numerical models. Water Resources Research 32.

932 Farrant, A.R., Smart, P.L., 2011. Role of sediment in speleogenesis; sedi-
933 mentation and paragenesis. Geomorphology 134, 79–93.

934 Ford, D.C., Williams, P., 2007. Karst Hydrogeology and Geomorphology.
935 John Wiley and Sons, Chichester, West Sussex, England.

936 Galdenzi, S., 2012. Corrosion of limestone tablets in sulfidic ground-water:
937 Measurements and speleogenetic implications. International Journal of
938 Speleology 41.

939 Goudie, A.S., Viles, H.A., 1999. The frequency and magnitude concept in
940 relation to rock weathering. Zeitschrift für Geomorphologie Supplement
941 Volumes , 175–189.

942 Groves, C.G., Meiman, J., 2005. Weathering, geomorphic work, and karst
943 landscape evolution in the Cave City groundwater basin, Mammoth Cave,
944 Kentucky. Geomorphology 67, 115–126.

945 Gulley, J., Martin, J., Moore, P., 2014. Vadose CO $_2$ gas drives dissolution
946 at water tables in eogenetic karst aquifers more than mixing dissolution.
947 Earth Surface Processes and Landforms 39, 1833–1846.

948 Gunn, J., 1982. Magnitude and frequency properties of dissolved solids trans-
949 port. Zeitschrift für Geomorphologie 26, 505–511.

950 Gunn, J., 2004. Encyclopedia of caves and karst science. Taylor & Francis,
951 New York, NY.

952 Helsel, D.R., Hirsch, R.M., 2002. Statistical methods in water resources. vol-
953 ume 323. Techniques of Water Resources Investigations, Book 4, Chapter
954 A3, U.S. Geological Survey.

955 Hibbard, K.A., Law, B.E., Reichstein, M., Sulzman, J., 2005. An analy-
956 sis of soil respiration across northern hemisphere temperate ecosystems.
957 Biogeochemistry 73, 29–70.

958 Jeannin, P.Y., Malard, A., Häuselmann, P., 2017. Effect of cave ventilation on
959 karst water chemographs, in: Renard, P., Bertrand, C. (Eds.), Eurokarst
960 2016, Springer, Neuchâtel, Switzerland. pp. 129–139.

961 Johnson, M., Billett, M., Dinsmore, K., Wallin, M., Dyson, K., Jassal, R.,
962 2010. Direct and continuous measurement of dissolved carbon dioxide in
963 freshwater aquatic systems - method and applications. Ecohydrology 3,
964 68–78.

965 Knierim, K., Pollock, E., Hays, P., Khojasteh, J., 2015a. Using Stable Iso-
966 topes of Carbon to Investigate the Seasonal Variation of Carbon Transfer

967 in a North-western Arkansas Cave. Journal of Cave and Karst Studies 77,
968 12–27.

969 Knierim, K.J., Hays, P.D., Bowman, D., 2015b. Quantifying the variability in
970 Escherichia coli throughout storm events at a karst spring in northwestern
971 Arkansas, United States. Environmental Earth Sciences 74, 4607–4623.

972 Knierim, K.J., Pollock, E.D., Covington, M.D., Hays, P.D., Brye, K.R., 2017.
973 Carbon cycling in the mantled karst of the Ozark Plateaus, central United
974 States. Geoderma Regional 10, 64–76.

975 Larock, B.E., Jeppson, R.W., Watters, G.Z., 2000. Hydraulics of pipeline
976 systems. CRC Press.

977 Lloyd, J., Taylor, J.A., 1994. On the Temperature Dependence of Soil Res-
978 piration. Functional Ecology 8, 315.

979 Luetscher, M., Jeannin, P.Y., 2004. Temperature distribution in karst sys-
980 tems: the role of air and water fluxes. Terra Nova 16, 344–350.

981 Luetscher, M., Lismonde, B., Jeannin, P.Y., 2008. Heat exchanges in the
982 heterothermic zone of a karst system: Monlesi cave, Swiss Jura Mountains.
983 Journal of Geophysical Research: Earth Surface 113, 1–13.

984 Mattey, D.P., Atkinson, T.C., Barker, J.A., Fisher, R., Latin, J.P., Durrell,
985 R., Ainsworth, M., 2016. Carbon dioxide, ground air and carbon cycling
986 in Gibraltar karst. Geochimica et Cosmochimica Acta 184, 88–113.

987 McFarland, J.D., 1998. Stratigraphic summary of Arkansas. volume 36.
988 Arkansas Geological Commission.

989 Palmer, A.N., 1991. Origin and morphology of limestone caves. Bull. Geol.
990 Soc. Am. 103, 1–21.

991 Palmer, A.N., 2007a. Cave Geology. Cave Books, Dayton, OH.

992 Palmer, A.N., 2007b. Variation in rates of karst processes. Acta Carsologica
993 36, 15–24.

994 Plummer, L., Wigley, T., Parkhurst, D.L., 1978. The Kinetics of Calcite
995 Dissolution in CO_2-Water Systems at 5° to 60° C and 0.0 to 1.0 ATM
996 CO_2. American Journal of Science 278, 179–216.

997 Pugh, A.L., Westerman, D.A., 2014. Mean annual, seasonal, and monthly
998 precipitation and runoff in Arkansas, 1951-2011. USGS Scientific Investi-
999 gations Report 5006, 40 p.

1000 Scanlon, B., Thrailkill, J., 1987. Chemical similarities among physically
1001 distinct spring types in a karst terrain. Journal of Hydrology 89, 259–279.

1002 Schmidt, K.H., 1985. Regional variation of mechanical and chemical denuda-
1003 tion, upper Colorado River Basin, U.S.A. Earth Surface Processes and
1004 Landforms 10, 497–508.

1005 Simms, M.J., 2004. Tortoises and hares: dissolution, erosion and isostasy in
1006 landscape evolution. Earth Surface Processes and Landforms 29, 477–494.

1007 Smith, D.L., Johnson, L., 2004. Vegetation-mediated changes in microclimate
1008 reduce soil respiration as woodlands expand into grasslands. Ecology 85,
1009 3348–3361.

1010 Spearman, C., 1904. The proof and measurement of association between two
1011 things. The American journal of psychology 100, 441.

1012 Spötl, C., Fairchild, I.J., Tooth, A.F., 2005. Cave air control on dripwater
1013 geochemistry, Obir Caves (Austria): Implications for speleothem deposi-
1014 tion in dynamically ventilated caves. Geochimica et Cosmochimica Acta
1015 69, 2451–2468.

1016 Troester, J., White, W.B., 1984. Seasonal fluctuations in the carbon dioxide
1017 partial pressure in a cave atmosphere. Water Resources Research 20, 153–
1018 156.

1019 U.S. Geological Survey, 2020. USGS water data for the Nation: U.S. Geolog-
1020 ical Survey National Water Information System database, accessed May
1021 19, 2020 at https://doi.org/10.5066/F7P55KJN.

1022 Vesper, D.J., White, W.B., 2004. Storm pulse chemographs of saturation
1023 index and carbon dioxide pressure: Implications for shifting recharge
1024 sources during storm events in the karst aquifer at Fort Campbell, Ken-
1025 tucky/Tennessee, USA. Hydrogeology Journal 12.

1026 Whipple, K.X., Hancock, G.S., Anderson, R.S., 2000. River incision into
1027 bedrock: Mechanics and relative efficacy of plucking, abrasion, and cavi-
1028 tation. Geological Society of America Bulletin 112, 490–503.

Wigley, T., Brown, M., 1976. The Physics of Caves, in: Ford, T., Cullingford, C. (Eds.), The Science of Speleology. Academic Press, New York, pp. 329–358.

Wolman, M.G., Miller, J.P., 1960. Magnitude and frequency of forces in geomorphic processes. The Journal of Geology 68, 54–74.

Wong, C.I., Banner, J.L., Musgrove, M., 2011. Seasonal dripwater Mg / Ca and Sr / Ca variations driven by cave ventilation : Implications for and modeling of speleothem paleoclimate records. Geochimica et Cosmochimica Acta 75, 3514–3529.

Wood, W.W., 1985. Origin of caves and other solution openings in the unsaturated (vadose) zone of carbonate rocks : A model for CO2 generation. Geology 13, 822–824.

Wood, W.W., Petraitis, M., 1984. Origin and Distribution of Carbon Dioxide in the Unsaturated Zone of the Southern High Plains of Texas. Water Resources Research 20, 1193–1208.

Worthington, S., Davies, G., Quinlan, J., 1992. Geochemistry of springs in temperate carbonate aquifers: recharge type explains most of the variation, in: Proceedings, Colloque dHydrologie en Pays Calcaire et en Milieu Fissuré (5th Neuchâtel, Switzerland). Annales Scientifique de l'Université de Bescancxon, Geologie–Mémoires Hors Série, pp. 341–347.

Young, H., 2018. Quantifying Carbon Dioxide Fluxes in the Air and Water in Blowing Springs Cave, Arkansas. M.S.. University of Arkansas. United States – Arkansas.